

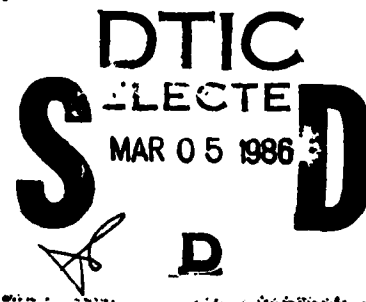
AD-A164 883

NSWC TR 83-246

DYNAMIC COMPACTION OF POROUS BEDS

BY H. W. SANDUSKY T. P. LIDDIARD
RESEARCH AND TECHNOLOGY DEPARTMENT

26 DECEMBER 1985



Approved for public release; distribution is unlimited.

DTIC FILE COPY



NAVAL SURFACE WEAPONS CENTER

Dahlgren, Virginia 22448-5000 • Silver Spring, Maryland 20903-5000

86 3 5 0 2 2

REPORT DOCUMENTATION PAGE

1a. REPORT SECURITY CLASSIFICATION UNCLASSIFIED			1b. RESTRICTIVE MARKINGS		
2a. SECURITY CLASSIFICATION AUTHORITY			3. DISTRIBUTION/AVAILABILITY OF REPORT Approved for public release, distribution unlimited.		
2b. DECLASSIFICATION/DOWNGRADING SCHEDULE					
4. PERFORMING ORGANIZATION REPORT NUMBER(S) NSWC TR 83-246			5. MONITORING ORGANIZATION REPORT NUMBER(S)		
6a. NAME OF PERFORMING ORGANIZATION Naval Surface Weapons Center		6b. OFFICE SYMBOL (If applicable) R13		7a. NAME OF MONITORING ORGANIZATION	
6c. ADDRESS (City, State, and ZIP Code) 10901 New Hampshire Avenue Silver Spring, Maryland 20903-5000			7b. ADDRESS (City, State, and ZIP Code)		
8a. NAME OF FUNDING / SPONSORING ORGANIZATION Naval Surface Weapons Center		8b. OFFICE SYMBOL (If applicable)		9. PROCUREMENT INSTRUMENT IDENTIFICATION NUMBER	
8c. ADDRESS (City, State, and ZIP Code) 10901 New Hampshire Avenue Silver Spring, Maryland 20903-5000			10. SOURCE OF FUNDING NUMBERS		
			PROGRAM ELEMENT NO. 61152N 62633W	PROJECT NO. ZR00001 SF33	WORK UNIT ACCESSION NO. R01AA202 R10BA433
11. TITLE (Include Security Classification) Dynamic Compaction of Porous Beds					
12. PERSONAL AUTHOR(S) Sandusky, H. W., and Liddiard, T. P.					
13a. TYPE OF REPORT Progress		13b. TIME COVERED FROM 5/81 TO 12/84		14. DATE OF REPORT (Year, Month, Day) 1985, December, 26	
15. PAGE COUNT 55					
16. SUPPLEMENTARY NOTATION					
17. COSATI CODES			18. SUBJECT TERMS (Continue on reverse if necessary and identify by block number)		
FIELD	GROUP	SUB-GROUP			
			Dynamic Compaction DDT		
			Porous Bed Compaction Wave Velocity		
			Deflagration-to-Detonation Transition Particle Velocity		
19. ABSTRACT (Continue on reverse if necessary and identify by block number) During the build-up of deflagration-to-detonation transition (DDT) in porous energetic materials, there is increasing dynamic compaction of the porous bed, which in turn affects the DDT build-up. To simulate the various pressures and pressurization rates that occur during DDT, a study of dynamic compaction was conducted with several different experimental arrangements, each designed to avoid direct ignition of the porous material by hot combustion products as in DDT. From those experiments, unreactive Hugoniot data were obtained for porous beds of three inert materials and a variety of energetic materials.					
20. DISTRIBUTION/AVAILABILITY OF ABSTRACT <input type="checkbox"/> UNCLASSIFIED/UNLIMITED <input checked="" type="checkbox"/> SAME AS RPT. <input type="checkbox"/> DTIC USERS			21. ABSTRACT SECURITY CLASSIFICATION Unclassified		
22a. NAME OF RESPONSIBLE INDIVIDUAL H. W. Sandusky			22b. TELEPHONE (Include Area Code) (202) 394-1612		22c. OFFICE SYMBOL R13

DD FORM 1473, 84 MAR

83 APR edition may be used until exhausted.
All other editions are obsolete

UNCLASSIFIED

★ U.S. Government Printing Office: 1985-639-013

0102-LF-014-6602

FOREWORD

Confid

The probability of deflagration-to-detonation transition (DDT) is known to increase considerably when the energetic material is porous; although, until recent experiments at this Center, it was neither appreciated nor predicted by existing models that there is extensive pore collapse during the buildup. Rather than study the details of pore collapse, the dynamic compaction of a collection of particles (a porous bed) was quantitatively measured by a variety of experimental techniques for several inerts, several single- and double-base propellants, two crystalline explosives, and two plastic-bonded explosives. When available, quasi-static compaction data from Wayne Elban and his coworkers, also of this Center, were compared with the dynamic data to determine rate effects. The work was accomplished for the Independent Research program, Task ZR01305, and the NAVSEA Explosive Block, Task SF33-337-691.

The authors thank Richard Bernecker for guiding and reviewing this work, Sig Jacobs for helpful suggestions concerning both the experimental techniques and the formulation of equations, Wayne Elban for his interest and help in integrating the quasi-static and dynamic data and for reviewing this report. The authors also are grateful to Carl Groves, Brian Glancy, Robert Baker, and Herman Gillum for assembling and instrumenting the experiments and then assisting in conducting them. The efforts of Bill Freeman in accurately machining the hardware and Nick Vogle in maintaining and occasionally building the electronic equipment are equally appreciated.

Approved by:

H. S. Haiss
H. S. HAISS, Acting Head
Energetic Materials Division



Accession For	
NTIS CRA&I	<input checked="" type="checkbox"/>
DTIC TAB	<input type="checkbox"/>
Unannounced	<input type="checkbox"/>
Justification	
By	
Distribution	
Availability Codes	
Distribution	Availability and/or Special
A-1	

CONTENTS

<u>Chapter</u>		<u>Page</u>
1	INTRODUCTION.....	1
2	EXPERIMENTAL TECHNIQUES AND RESULTS.....	3
	GAS DRIVEN COMPACTION EXPERIMENTS.....	5
	PISTON DRIVEN COMPACTION EXPERIMENTS.....	12
	RAMP LOADED COMPACTION EXPERIMENT.....	20
	SHOCK DRIVEN COMPACTION EXPERIMENTS.....	25
3	DISCUSSION.....	30
4	SUMMARY AND CONCLUSIONS.....	40
	REFERENCES.....	41
	NOMENCLATURE.....	43
	DISTRIBUTION.....	(1)

ILLUSTRATIONS

<u>Figure</u>		<u>Page</u>
1	SCHEMATIC OF APPARATUS FOR GAS DRIVEN COMPACTION.....	6
2	COMPACTION OF 60.0% TMD (1.383 g/cm^3) TEFLON 7C, SHOT CGC-10, IN GAS DRIVEN COMPACTION APPARATUS.....	10
3	SCHEMATIC OF APPARATUS FOR PISTON DRIVEN COMPACTION.....	13
4	SCHEMATIC OF MODIFIED APPARATUS FOR PISTON DRIVEN COMPACTION.....	14
5	SCHEMATIC OF PDC TEST SECTION FOR INTERMEDIATE CONFINEMENT.....	16
6	RADIOGRAPHIC DATA FROM SHOT PDC-41B: DISPLACEMENT OF TRACERS VERSUS THEIR ORIGINAL POSITION.....	19
7	PERCENT STRAIN OF LEXAN TUBE CIRCUMFERENCE AT 63.5 mm VERSUS TIME DURING COMPACTION OF CLASS D HMX.....	21
8	RAMP PRESSURE GENERATOR USED TO COMPACT TEFLON 7C POWDER.....	22
9	DISTANCE-TIME TRACES OBTAINED FROM PMMA OPTICAL DISKS IN 60.1% TMD TEFLON 7C USING THE RAMP PRESSURE GENERATOR, SHOT JK-054.....	24
10	GAP TEST ARRANGEMENT USED TO RECORD PARTICLE MOTION IN POROUS MATERIAL BY LIGHT TRANSMITTED THROUGH OPTICAL DISKS.....	26
11	DISTANCE-TIME TRACES OBTAINED FROM RTV OPTICAL DISKS IN LOW DENSITY SUCROSE USING GAP TEST ARRANGEMENT, SHOT JK-048.....	27
12	DISTANCE-TIME TRACES OBTAINED FROM PMMA OPTICAL DISKS IN 60% TMD TEFLON 7C USING GAP TEST ARRANGEMENT, SHOT JK-056.....	29
13	COMPACTION DATA FOR INERT MATERIALS.....	33
14	COMPACTION DATA FOR A. SINGLE- AND B. DOUBLE-BASE PROPELLANTS.....	35
15	COMPACTION DATA FOR CLASS D HMX.....	36
16	PRESSURE VERSUS PARTICLE VELOCITY FOR PISTON DRIVEN COMPACTION OF 75% TMD BEDS OF A. PBXW-108(E) AND B. PBXW-109(E).....	39

TABLES

<u>Table</u>		<u>Page</u>
1	GRANULAR MATERIALS FOR DYNAMIC COMPACTION STUDIES.....	4
2	SUMMARY OF GAS DRIVEN COMPACTION EXPERIMENTS.....	8
3	SUMMARY OF PISTON DRIVEN COMPACTION EXPERIMENTS.....	17
4	SUMMARY OF NON-PBX COMPACTION DATA WITH SUGGESTED CORRECTIONS FOR LEXAN TUBE EXPANSION.....	31
5	SUMMARY OF PBX COMPACTION DATA WITH SUGGESTED CORRECTIONS FOR LEXAN TUBE EXPANSION.....	37

CHAPTER 1

INTRODUCTION

Compaction of highly porous beds of explosives and propellants has been observed to be extensive in experimental studies of deflagration to detonation transition (DDT).¹⁻³ The compaction occurs in stages corresponding to those for the accelerating reaction and pressure buildup in the DDT mechanism; compaction during each stage affects the reaction process in each subsequent stage. The stages of the DDT mechanism and the compaction processes occurring during those stages can be summarized as 1) the pre-ignition stage during which the pressure from the hot gas ignition source drives a weak compaction wave into the porous bed for often hundreds of microseconds before the energetic material ignites, 2) the conductive/convective burning stage during which the increasing pressure buildup at the ignited end of the bed continuously drives compressive waves into the porous bed, forming a strong compressive wave at some depth in the porous bed, 3) the compressive burning stage during which reaction is initiated via rapid pore collapse from the strong compressive wave, and 4) the shock-to-detonation transition (SDT) which results from the rapidly strengthening compaction/shock front, driven by compressive burning. Note that a compaction front (compressive wave) of increasing strength, first driven by conductive/convective burning, initiates the final two stages of the DDT mechanism. But even the partial collapse of pores by pre-ignition compaction subsequently effects convective ignition in the next stage and compressive reaction in the final stages.

An understanding of DDT for very porous energetic materials, and the ability to model it numerically, obviously requires knowledge of compaction processes. Therefore, it was decided that dynamic and quasi-static measurements of compaction would be made over a pressure range appropriate for DDT buildup. Materials that were to be compacted included inert simulants for energetic materials, single- and double-base propellants (smokeless powders for firearms), and plastic-bonded as well as crystalline explosives.

It was necessary to develop several dynamic compaction techniques in order to simulate the range of pressures, as well as pressurization rates, appropriate for DDT buildup. Initially, pre-ignition compaction by the ignitor used in DDT experiments at NSWC was studied for two inert simulants in order to avoid the complications associated with reaction of the compacting material.^{4,5} In subsequent experimental techniques, the energetic materials were compacted without contact with hot combustion products in order to avoid direct ignition. However, as the driving pressure was increased, the energetic materials experienced compressive reaction and its growth, much like that during the final stages of DDT. The threshold for compressive reaction has been found to correlate approximately with the particle velocity in the compacted region;

that threshold was 73-151 m/s for several of the materials reported here.⁶ Both near and beyond that threshold for a particular material, the compaction process would be influenced by compressive reaction and its growth.

Quasi-static compaction, in contrast to high strain-rate dynamic compaction, does not induce compressive reaction. In addition, quasi-static data can be generated relatively quickly and economically. W. Elban and coworkers have quasi-statically compacted two inert simulants,^{4,7,8} several single- and double-base propellants,^{8,9} and coarse HMX explosive.¹⁰ However, for that data to be useful in describing the dynamic compaction during DDT, an assessment of strain rate effects is required. A simple comparison of dynamic and quasi-static data provided such an assessment for the above materials;⁸ better yet, observed rate effects in an inert¹¹ and in an explosive¹² were predicted from stress relaxation measurements following their quasi-static compaction. The quasi-static measurements have been incorporated in DDT models under development by K. Kim^{4,13} at NSWC and C. Price and T. Boggs¹⁴ at NWC.

This report describes in detail the various dynamic compaction techniques which were developed subsequent to the ignitor driven compaction experiments.^{4,5} These techniques involved 1) rapid pressurization by an inert gas at room temperature, 2) impact by a long rod, 3) acceleration of a piston in contact with the material, and 4) the attenuated shock from a detonating explosive. Particle velocity, compaction front velocity, and density of the compacted material were measured by photographic and radiographic techniques. The density of the compacted material, as well as the pressure required to compact it, were calculated from the particle and compaction front velocities using jump equations. Confidence in the suitability of jump equations for these calculations was based on the agreement between the measured and calculated densities for compacted material. The calculated parameters were then compared with the corresponding quasi-static data, whenever possible. The reported dynamic data are presumably unaffected by compressive reaction; observations pertaining to the onset and growth of compressive reaction during dynamic compaction are discussed elsewhere.^{15,16}

CHAPTER 2

EXPERIMENTAL TECHNIQUES AND RESULTS

Simulation of the wide range of pressures and pressurization rates observed during DDT buildup required several different experimental arrangements. For the pre-ignition stage, porous beds of inert granular materials were confined by the same Lexan tube arrangement used in some NSWC DDT studies. The beds were compacted by the gas products of an ignitor usually used in DDT studies; the use of inert beds avoided complications from porous bed reaction, except for possible pyrolysis. This ignitor driven compaction (IDC) is described elsewhere.^{4,5} The following experimental arrangements, which are described in this report, were designed to compact energetic materials without direct ignition. To simulate the early stages of DDT--pre-ignition and the onset of conductive/convective burning--the porous bed was loaded by the sudden release of nitrogen from a closely coupled reservoir at room temperature. This is referred to as gas driven or cold gas compaction (CGC). As the final stages of DDT--compressive burning and SDT--are approached, a region of extensively compacted bed between the combustion zone and the compaction front acts much like a piston. This was simulated by the piston driven compaction (PDC) apparatus, which drives a long rod into the porous bed, generating pressures of up to 200 MPa for $>200 \mu s$. The CGC and PDC apparatuses maintain an approximately constant pressure on the porous bed during the experiment, which is convenient for data analysis. In order to simulate the ramp loaded compaction (RLC) that occurs during buildup to DDT, a Teflon plug was accelerated into the bed by confined product gases from detonating a long strip of explosive.* A final arrangement, which used a gap test donor, was for studying the shock driven compaction (SDC) which occurs during the final stage of DDT.

A description of the granular materials and the different techniques used to compact each material are listed in Table 1. The inert materials--Teflon 7C, melamine, and sugar--were chosen to represent variations in mechanical properties encountered for a variety of energetic materials. The energetic materials cited were chosen because of their use in DDT and/or SDT studies at NSWC.

For most experiments the compaction parameters measured were particle velocity (u), compaction front velocity (U), and density of the compacted material (ρ_c). The compaction pressure is difficult to measure

*L. Green¹ at LLNL has also studied the response of porous beds to ramp loading.

TABLE 1. GRANULAR MATERIALS FOR DYNAMIC COMPACTION STUDIES

<u>Material</u> *	<u>Ingredients</u> *	<u>TMD</u> ** (g/cm ³)	<u>δ</u> [†] (μ m)	<u>Experiments</u> ^{††}
Inert:				
Teflon 7C	--	2.305	30 ⁷	CGC, PDC, RLC, SDC
Melamine	--	1.573	46-56 ⁷	PDC
Table sugar	Sucrose	1.588	Random	SDC
Ball Propellants:				
WC 140	NC	1.65	411 ⁹ (spherical)	CGC
Fluid A	NC	1.65	34 ⁹ (spherical)	CGC
TS 3660	NC/12% NG	1.64	714 ⁹ (spherical)	CGC
WC 231	NC/25% NG	1.64	790 ⁹ (rolled)	CGC, PDC
Explosives:				
Class D HMX	--	1.90	870 ¹⁰	PDC
Tetryl (NSWC X812)	--	1.73	470 ¹⁸	PDC
PBXW-108(E)	RDX/Binder	1.555	2170 (cubes)	PDC
PBXW-109(E)	RDX/Al/Binder	1.655	2170 (cubes)	PDC

*Material/Ingredients

NC = Nitrocellulose

NG = Nitroglycerin

HMX = Cyclotetramethylenetetranitramine

RDX = Cyclotrimethylenetrinitramine

Al = Aluminum

**TMD = Theoretical maximum density

[†] δ = Average particle size

(When available, particle size analyses are referenced.)

††Experiments

CGC = Gas driven compaction (cold gas compaction)

PDC = Piston driven compaction

RLC = Ramp loaded compaction

SDC = Shock driven compaction

directly and often does not correspond to the measurable radial pressure on the inner wall; therefore, jump condition calculations for pressure (p_h) are tabulated with the measurements. Although jump condition calculations apply for a steady state process, whereas experimental conditions were in reality quasi-steady, the calculations for density (ρ_h) behind each compaction front consistently agreed with measurements.

There was never evidence of a two (elastic/plastic) wave structure during the experiments, probably because the hand loaded beds, except for perhaps the propellants, were unable to support any significant elastic load. Even if there was an elastic wave, the small displacements associated with it were unlikely to be resolved from the experimental measurements. The material ahead of a compaction wave was at rest ($u_0 = 0$) and at its original packing density (ρ_0). Assuming a single wave, the jump condition equations therefore are

$$\rho_h = \frac{\rho_0 U}{U-u} ,$$

$$p_h = p_0 + \rho_0 U u .$$

Since there was no significant residual pressure on the beds from the packing process, a p_0 of 0.1 MPa (atmospheric pressure) was used in the calculations.

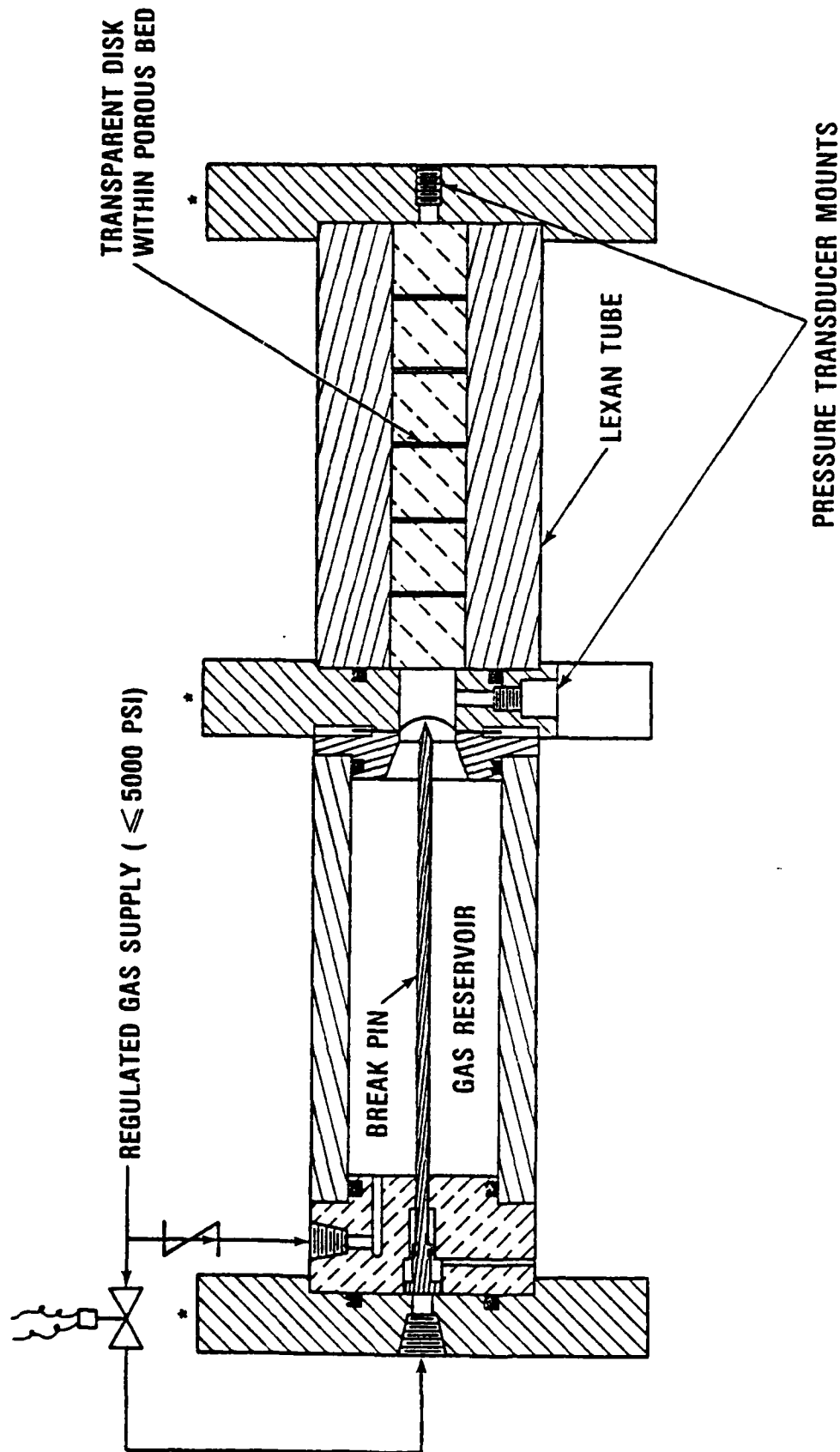
All of the bed densities reported have been non-dimensionalized by converting them to percent theoretical maximum density (%TMD = 100 ρ /TMD). This parameter is equivalent to the volume percentage of the bed occupied by the solid, if the solid itself is not compressed. For most experiments, there was insignificant bulk compression of the solid; however, as will be discussed, the PBXs incurred a small amount of compression at the highest pressures. The above jump equations thus become

$$\%TMD_h = \frac{\%TMD_0 U}{U-u} , \quad (1)$$

$$p_h = p_0 + \frac{\%TMD_0}{100} TMD U u . \quad (2)$$

GAS DRIVEN COMPACTION EXPERIMENTS

Porous beds of Teflon 7C and several single- and double-base propellants were compacted through the sudden release of room temperature nitrogen from a reservoir that had been pressurized to ≤ 27.7 MPa (4000 psi). As shown in Figure 1, the reservoir is closely coupled to the porous bed in order to achieve a pressurization rate typical of the early stages of DDT. An experiment is initiated by pneumatically driving a pin into the diaphragm which seals the orifice between the reservoir and the porous bed. The four-cornered pin promotes the rupturing of the diaphragm into four petals; they remain attached to the clamped annulus of the diaphragm and thus avoid complications from impact of petal fragments on the porous bed. The 19 mm diameter of the orifice is somewhat less than the 25.4 mm diameter of the porous bed in order to permit relatively uniform pressurization of the bed while avoiding preferential gas flow along the interface between the bed and the confining tube, as was observed



* PLATES CONNECTED BY BOLTS, NOT SHOWN.

FIGURE 1. SCHEMATIC OF APPARATUS FOR GAS DRIVEN COMPACTION

in the IDC experiments.⁵ The confining tube of Lexan is a standard plastic NSWC DDT tube,² usually shortened to a length of 146 mm.

Obtaining a suitable diaphragm arrangement required some trial and error, and therefore is reported in detail. The 38.1 mm diameter diaphragms of brass shim stock had thicknesses of 0.15, 0.20, and 0.41 mm for reservoir pressures of 7.0, 13.9, and 27.7 MPa, respectively. The brass disks were not scored to promote controlled rupturing; however, they were prepressurized (and thus dimpled) without the break pin in place, in order to use a break pin that protrudes past the clamped portion of the diaphragms. When using the shorter break pin with initially undimpled diaphragms, the 7.1 mm stroke of the break pin was inadequate to rupture the diaphragms reliably. The diaphragms were sandwiched between two pieces of gasket material; the upstream (reservoir) gasket had a 20.3 mm opening, whereas the downstream gasket had a 17.8 mm opening, which is slightly smaller than the 19.0 mm diameter orifice, in order to protect the diaphragm from being cut by the edge of the orifice. The edge of the orifice had a 0.6 mm radius to reduce its tendency to cut, but a larger radius may have been more appropriate. The gaskets were initially made from 0.8 mm thick material of pressed fiber obtained from Fibreflex Packing and Mfg. Co., Phila., PA. Toward the end of the study, the downstream gaskets were made from 0.6 mm thick, annealed copper in order to increase their durability.

The experiments were instrumented for measurements of pressure and bed motion. The gas pressure driving the compaction was measured by a piezoelectric transducer at the orifice between the reservoir and the bed; also, a piezoelectric transducer was usually mounted at the far end of the bed. Bed motion was obtained by backlighting the apparatus with a xenon flash and photographing the transmitted light through transparent disks in the bed, usually at 25.4 mm increments. The major advantage of this technique, as compared to flash radiography of metallic tracers in the bed, is that bed motion at each disk can be recorded continuously with a streak camera whereas flash radiographs are obtained at a few (2-4) distinct times. Unfortunately, the disks disrupt the compaction process, as will be shown. The transparent disk technique was suggested by S. J. Jacobs of NSWC and first demonstrated by L. Green of LLNL.¹⁷

The gas driven compaction data are summarized in Table 2. The CGC prefix for the shot numbers corresponds to cold gas compaction, in contrast to the hot ignitor products in the previous IDC experiments. In Table 2, the values for u are based on the motion of the first disk in the bed, while values for $\%TMD_c$ are based on the reduced separation between the first pair of disks. As will be shown, each value for U is an average over the entire bed length. Some of the values for $\%TMD_f$ are based on the average separation of the disks after the experiment was completed and the apparatus depressurized; therefore, the bed was elastically unloaded and at a reduced density. The preferred measurements of $\%TMD_f$ were based on disk separations just after the reflection of the compaction front at the far end before the apparatus was depressurized. For Teflon 70 the difference between the two measurements was relatively small, indicating primarily plastic deformation of the bed; however, for the one WC 140 experiment (Shot CGC-12) with both measurements of $\%TMD_f$, the relatively large difference suggests that the deformation was primarily elastic.

TABLE 2. SUMMARY OF GAS DRIVEN COMPACTION EXPERIMENTS

INITIAL CONDITIONS*					OBSERVATIONS*					CALCULATIONS*				
SHOT NO.	POROUS BED MATERIAL	ΣTMD_0	DISKS		L (mm)	P_r (MPa)	P_{GAS} (MPa)	P_L (MPa)	$\frac{u}{U}$ (mm/ μ s)	$\frac{u}{U}$ (mm/ μ s)	ΣTMD_c	ΣTMD_f	P_h (MPa)	
			TYPE	$\frac{x_1}{x_2}$ (mm)										
CGC-4			RTV	25.4		7.0	7.3	0.8	-	-	-	80.2 ^b		
-5			-	-		7.0	6.6	1.9	-	-	-	75.8 ^b		
-6			RTV	25.4		13.9	13.4	19.9	0.038	0.162	80.3	88.0 ^b , 92.1 ^c	78.4	8.6
-7	Teflon 7C	60.0	-	-	139.7	13.9	12.5	39.9	-	-	-	88.4 ^b		
-9			PMMA	25.4		13.9	13.2	38.8	0.049	0.182	82.9	89.9 ^b , 92.2 ^c	82.1	12.4
-10			PMMA	0.0		13.9	13.2	29.0	0.047	0.160	86.3	90.3 ^b , 91.6 ^c	85.0	10.5
-8			-	-		27.7	19.5	85.1	-	-	-	94.8 ^b		
-12				0.0		13.9	14.6	17.9	0.030	0.38	65.7	62.2 ^b , 68.1 ^c	65.1	11.4
-13	WC 140	60.0	PMMA	0.0	139.7	27.7	25.2	37.5	0.050	0.46	67.3	75.0 ^c	67.3	22.9
-14				38.1		27.7	24.5	40.8	0.045	0.40	67.4	76.0 ^c	67.6	17.9
-16	TS 3660	57.6	PMMA	25.4	139.7	13.9	13.3	18.0	0.032	0.343	62.7	68.3 ^c	63.6	10.5
-17						27.7	21.1	32.9	0.050	0.369	66.8	75.6 ^c	66.7	17.5
-18	Fluid A	60.6	PMMA	25.4	139.7	13.9	14.9	1.7	-0.024 ^a	0.26	-	-	66.8	6.3
-19			PMMA&RTV			27.7	25.1	31.4	-0.032 ^a	0.32	-	-	67.3	10.3
-22	WC 231	50.0	PMMA	25.4	139.7	27.7	19.5	-	0.085	0.277	72.7	88.0 ^c	72.1	19.4
-23		49.4			292.1	27.7	16.1	-	0.073	0.251	72.4	-	69.6	14.9

* ΣTMD_0 = Initial volume percentage of solid in bed x_1 = Location of the first disk L = Initial length of porous bed including disks except for a driven end disk P_r = Initial reservoir pressure P_{GAS} = Average gas pressure on the driven end P_L = Pressure of reflected compaction wave at $x = L$ u = Particle velocity behind compaction front

a. Film images of disks were very weak

 U = Compaction front velocity ΣTMD_C = Measured volume percentage of solid behind the compaction front ΣTMD_f = Final volume percentage of bed occupied by solid

b. After depressurization of the bed

c. Just after reflection of compaction front

 ΣTMD_h = Jump condition calculation for volume percentage of solid behind the compaction front P_h = Jump condition calculation for compaction front pressure

The pressure transducer measurements in Figure 2a and the streak camera record of transparent disk motion in Figure 2b illustrate the data obtained with this apparatus. The transducer near the driven end of the bed ($x = -15$ mm) first senses a pressure of 2.5 MPa from the gas flowing toward the bed, just after the diaphragm ruptures. The subsequent pressure rise to 13.2 MPa (p_{GAS} in Table 2) is from the retardation of the gas flow by the compacting bed. This compaction pressure slowly declines up to 1250 μs as the compacting bed increases the gas volume. Then the reflected compaction front from the far end arrests any further bed motion. The arrival of the compaction front at the far end and the propagation of the reflected wave back to the driven end are indicated by the rapid rise in pressure by the far end transducer. The peak pressure of 29.0 MPa at the far end (p_{f} in Table 2) is assumed to be characteristic of the rearward wave that both arrests the bed motion and further compacts the bed.

In Figure 2b the initial movement of the disks indicates arrival of the compaction front, and the rate of disk movement is equivalent to the particle velocity of the compacted bed. Usually the particle velocity declines with increasing distance from the driven end, whereas the compaction front velocity appears to remain steady (within experimental error). The decrease in particle velocity can be attributed to wall friction as well as to the reduction in driving pressure. Particle and compaction front velocities behaved similarly in the IDC experiments; it was calculated that the particle velocity was more sensitive to pressure than the compaction front velocity,⁵ which may explain why the compaction front velocity does not appear to decline. In Figure 2b, the extrapolation of the compaction front to the driven end is denoted by the symbol (\square), and to the far end by symbol (Δ). The same symbols are plotted in Figure 2a; the symbol (\square) for the onset of compaction precedes the major response of the driven end transducer because it is mounted ~ 15 mm from the end of the bed. The symbol (Δ) for reflection of the compaction front at the far end corresponds to the onset of rapid pressurization. In Figure 2b, the arrested motion of the last two disks is caused by the rearward wave. Although this was more clearly seen in other experiments, the change in disk velocity was generally not distinct enough to define the velocity of the rearward wave.

Compaction values obtained from jump condition calculations ($\%TMD_{\text{p}}$ in Table 2) show reasonable agreement with experimental measurements ($\%TMD_{\text{c}}$), the differences being an indication of experimental accuracy. Calculated pressures (p_{H}) are in reasonable agreement with gas pressures exerted on the beds (p_{GAS}), specifically for those experiments with little drag on the inner tube wall. As elaborated in following discussions, there appeared to be significant wall drag for shots involving RTV disks or a bed of Fluid A powder.

A number of experiments with Teflon 7C, packed at 60.0% TMD (1.383 g/cm^3) were conducted in order to test the apparatus and to determine the effect of the transparent disks on the compaction process. Two types of disks were used. Pliable disks were cut from a cast sheet of General Electric's RTV 615 (1.6 or 1.0 mm thick); more rigid PMMA disks were machined from 2.2 mm or 0.6-0.8 mm thick sheets. The RTV 615 was first chosen as a disk material since pressure exerted on the faces of a disk causes it to wet the inner wall of the tube, thereby allowing good transmission of the backlighting. However, the good

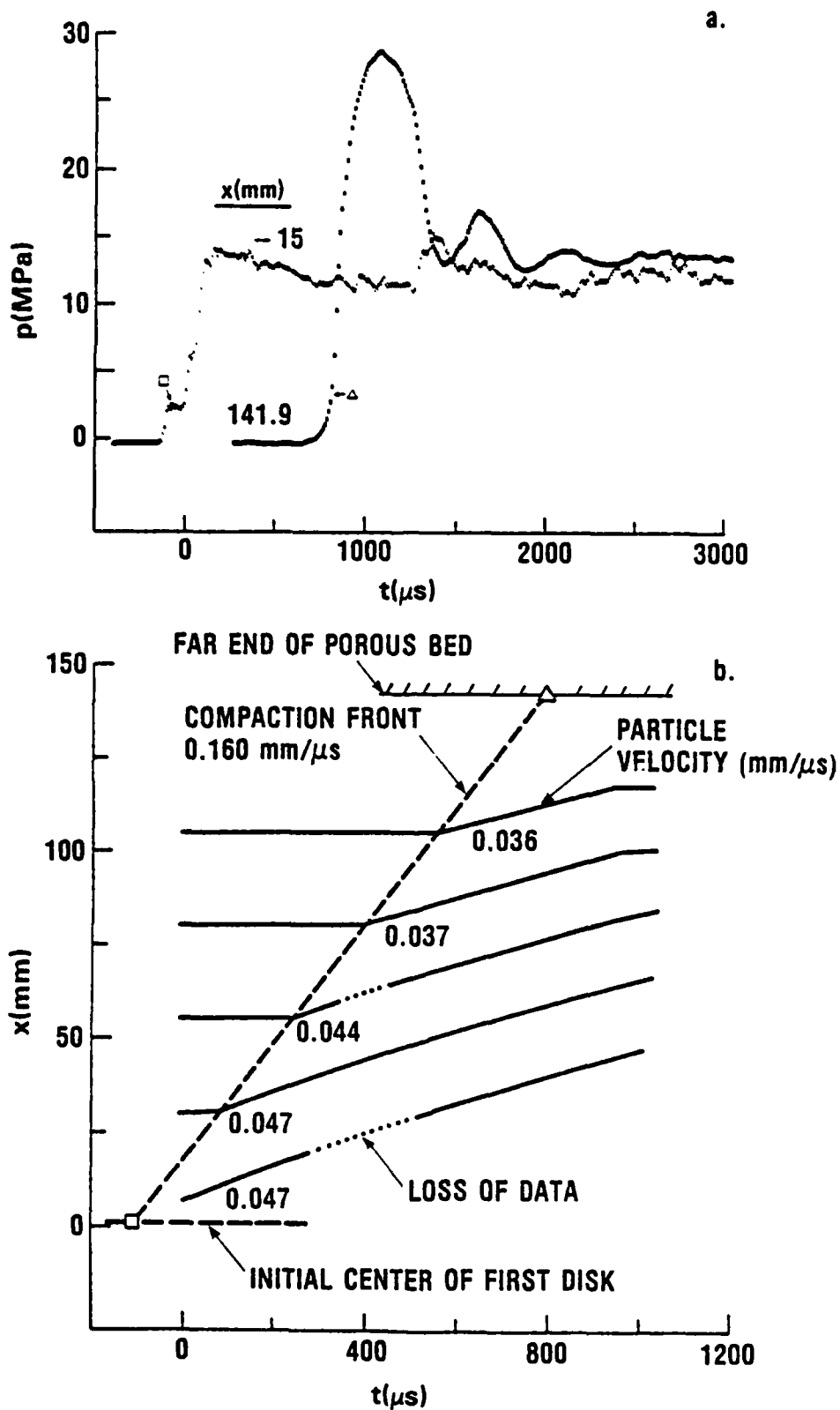


FIGURE 2. COMPACTION OF 60.0% TMD (1.383 g/cm^3) TEFLON 7C, SHOT CGC-10, IN GAS DRIVEN COMPACTION APPARATUS. a. PRESSURE TRANSDUCER RESPONSES, b. DISK PATHS FROM STREAK CAMERA FILM

contact with the inner tube wall caused considerable drag and, therefore, loss of transmitted pressure along the length of the bed. This can be seen in Table 2 by comparing the pressures (P_L) at the far-end transducer for similar driving pressures (P_{GAS}) on beds with RTV disks and without any disks. For example, when $P_{GAS} = 7$ MPa, the peak pressure at the far end of a bed containing four 1.6 mm thick RTV disks (Shot CGC-4) was less than half of the far-end pressure in a bed without disks (Shot CGC-5). A similar result was observed for $P_{GAS} = 13-14$ MPa (compare Shots CGC-6 and 7), whereas inclusion of 2.2 mm thick PMMA disks in Shot CGC-9 resulted in very little wall drag. Therefore, in subsequent tests PMMA disks were used, and following Shot CGC-14 the disk thickness was decreased to 0.6-0.8 mm in order to further reduce disturbance of the compaction process.

The effect that gas flow into the bed has on the compaction process was investigated for both Teflon 7C and WC 140. Gas flow was most restricted in Shots CGC-10 and 13 by a disk on the end of the bed, whereas gas flow was permitted at least 25.4 mm into the beds for Shots CGC-9 and 14 before restriction by a disk. The observed effects on compaction of Teflon 7C and WC 140 differed, but were small enough to be within the range of the statistical nature of porous beds and experimental error.

As mentioned in the Introduction, compressive reaction can occur from the rapid particle deformation during dynamic compaction. In Shot CGC-13 the WC 140 powder reacted no sooner than 4 ms after the beginning of the compaction process. By this time the pressures in the apparatus were nearly equalized. Rather than ascribe such a delayed reaction to the compaction process, it is assumed that the reaction was initiated by ball powder pinched between the junction plate and the Lexan tube, since pinched grains were recovered from the next test (Shot CGC-14). The formation of a gap at the plate/tube interface resulted from 1) stretching of the 19 mm diameter threaded rods which clamp the tube to the plate and 2) a reduction of the tube length as a consequence of the interior tube pressure. Pinching should occur when the tube and plates snap back together after the decline of the high dynamic pressures. For experiments following Shot CGC-14, rod stretching was essentially eliminated by replacing the 19.0 mm diameter threaded rods of mild steel with 25.4 mm diameter hardened steel bolts. Although there was still evidence of porous bed particles trapped between the tube and plates, reaction did not occur in the porous beds of Fluid A and TS 3660. The absence of reaction in TS 3660 is notable since it contains 12.3% NG and, therefore, should be more reactive than both of the nitrocellulose powders, assuming that other factors such as particle size are not controlling. However, there apparently was compaction initiated reaction in the WC 231 experiments. The data for WC 231 in Table 2 were obtained prior to ignition and are probably only insignificantly affected by the buildup of reaction prior to ignition.

Of the materials that were compacted dynamically, only recovered samples of TS 3660 were evaluated via photomicrographs by W. Elban. The extent of particle deformation in Shots CGC-16 and 17 was similar to that for quasi-static compaction to about the same stress levels.⁹ This indicates that the compaction mechanism at low stress levels was not significantly altered by a substantial increase in the rate of compaction (roughly five orders of magnitude).

The transparent disk technique was not effective for recording bed motion in the Fluid A propellant used in Shots CGC-18 and 19. Fine particles between the edges of both types of disks and the inner tube wall resulted in film images that were barely visible prior to compaction and persisted for less than 100 μ s following arrival of the compaction front. The nearly equal values for the calculated compaction in Shots CGC-18 and 19, despite significantly different driving pressures, are shown in the Discussion section to be representative of the quasi-static compaction data in this pressure range. Also, for Shot CGC-18 it appears from the attenuation of pressure between the driven end, 15.4 MPa, and the far end, 1.7 MPa, that powder caught between the PMMA disks and inner tube wall increased the drag of the disks considerably. In subsequent experiments with such fine powders, flash radiography was utilized to record bed motion.

PISTON DRIVEN COMPACTION EXPERIMENTS

The PDC experiment, like the CGC experiment, is designed to preclude porous bed reaction by any source other than high strain rate deformation from porous bed compaction. The schematic of the original apparatus in Figure 3 shows basically a powder gun for launching a 25.4 mm diameter x 305 mm long Lexan piston into a porous bed, which is confined laterally by a Lexan tube. The Lexan tube is identical to that used in the previous CGC experiments, except for the machining on one end for attaching it to the barrel. End plates, which are connected by long bolts, clamp the Lexan tube to the steel barrel. The piston is driven by the combustion products of a B/ KNO_3 ignitor and up to 3.4 grams of WC 231 reloading powder. The velocity of the piston just prior to impacting the porous bed (v_p) is experimentally related to the mass (m) of the WC 231 powder according to $v_p(\text{m/s}) = 70 + 63.3 m(\text{g})$, with a variation of ± 10 m/s. Slots through the steel/Lexan joint provide openings for: 1) venting air between the piston and porous bed, 2) observing the backlit piston prior to and following piston impact of the porous bed, and 3) inserting a trigger pin in the piston path. The tip of the trigger pin is pushed away by the piston, instead of being sheared off and then driven into the porous bed; the contact of the pin by the piston turns on the xenon flash for backlighting the piston and triggers any other instrumentation. In order to observe piston motion even after bed impact, the first ~35 mm of the piston is polished and then circumferentially scribed at several locations in order to interrupt the backlighting at those locations.

The apparatus was modified following Shot PDC-15 because of damage to the end of the barrel from several detonations in the porous beds. The assembly drawing of the apparatus in Figure 4 shows these modifications as well as the actual vertical orientation of the apparatus during an experiment. The damaged end of the barrel was removed and the new end was threaded for a replaceable barrel extender. A 25.4 mm thick steel plate at the muzzle end of the barrel further protects it from violent reactions. Slots in the steel/Lexan joint in the original apparatus were shifted entirely to the barrel extender in order to avoid stress cracks which developed in the slotted Lexan tubes. An additional trigger pin was added to assure that the xenon flash for backlighting is turned on before the piston reaches the slots in the barrel extender.

Lexan confinement tubes were suitable for both photographic and flash radiographic instrumentation, which was particularly helpful for observing

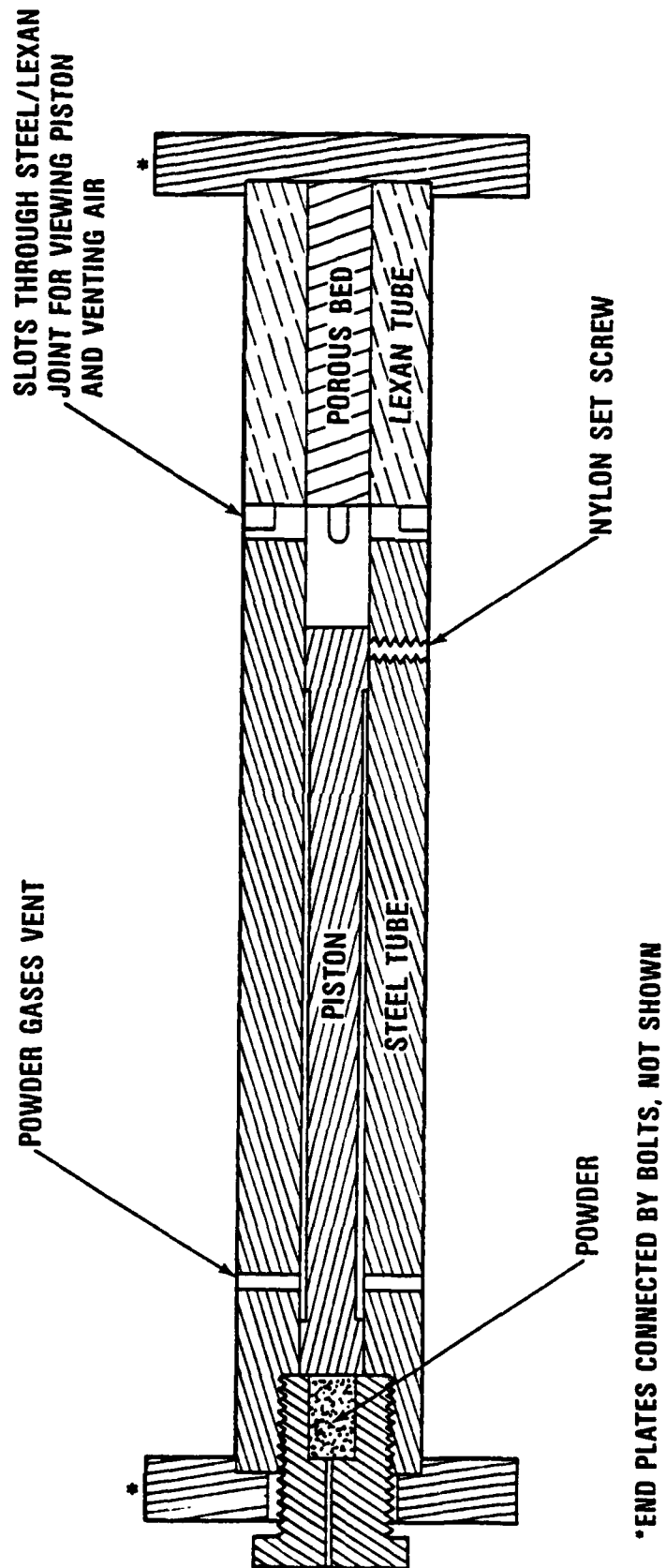


FIGURE 3. SCHEMATIC OF APPARATUS FOR PISTON DRIVEN COMPACTION

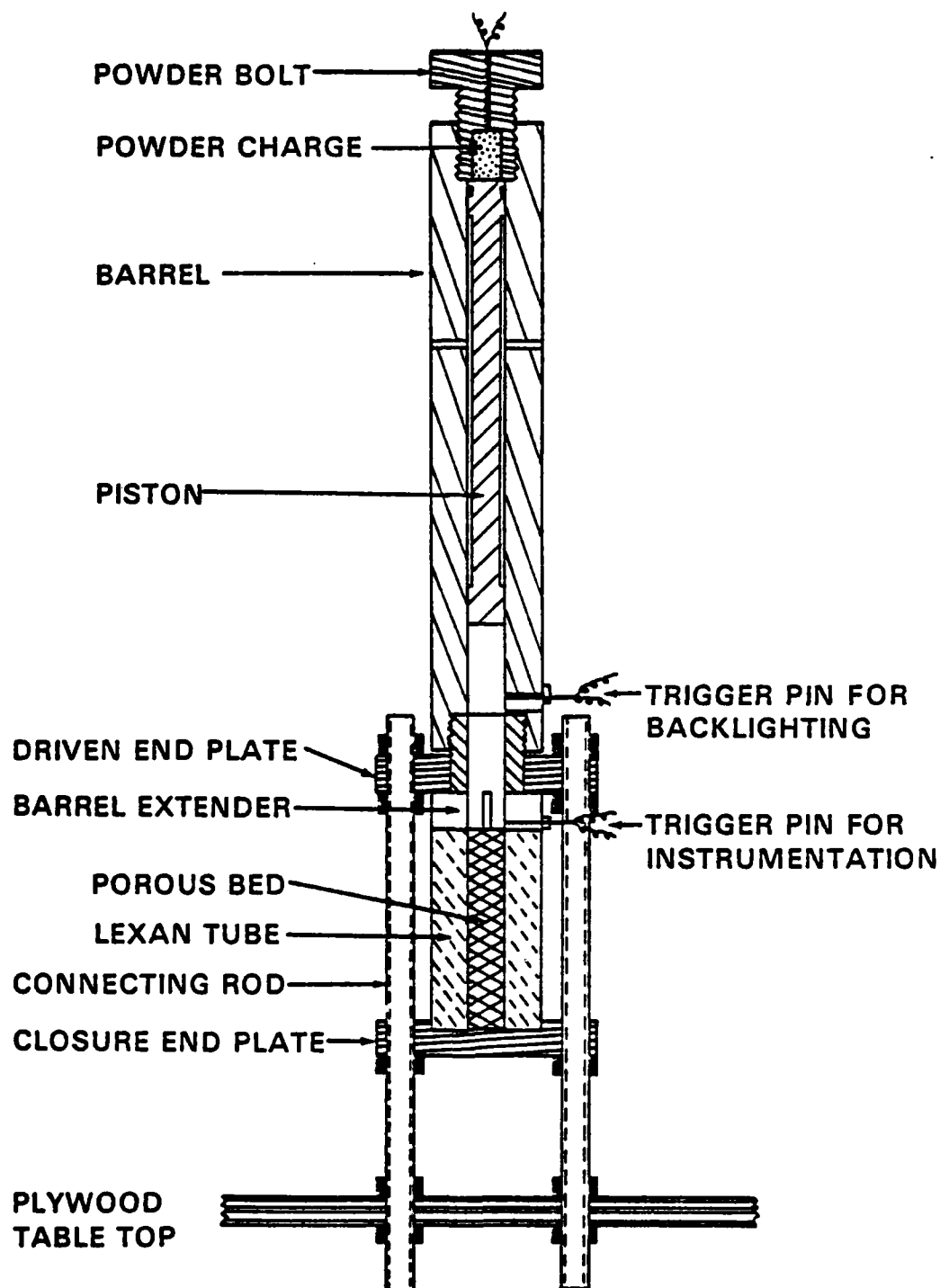


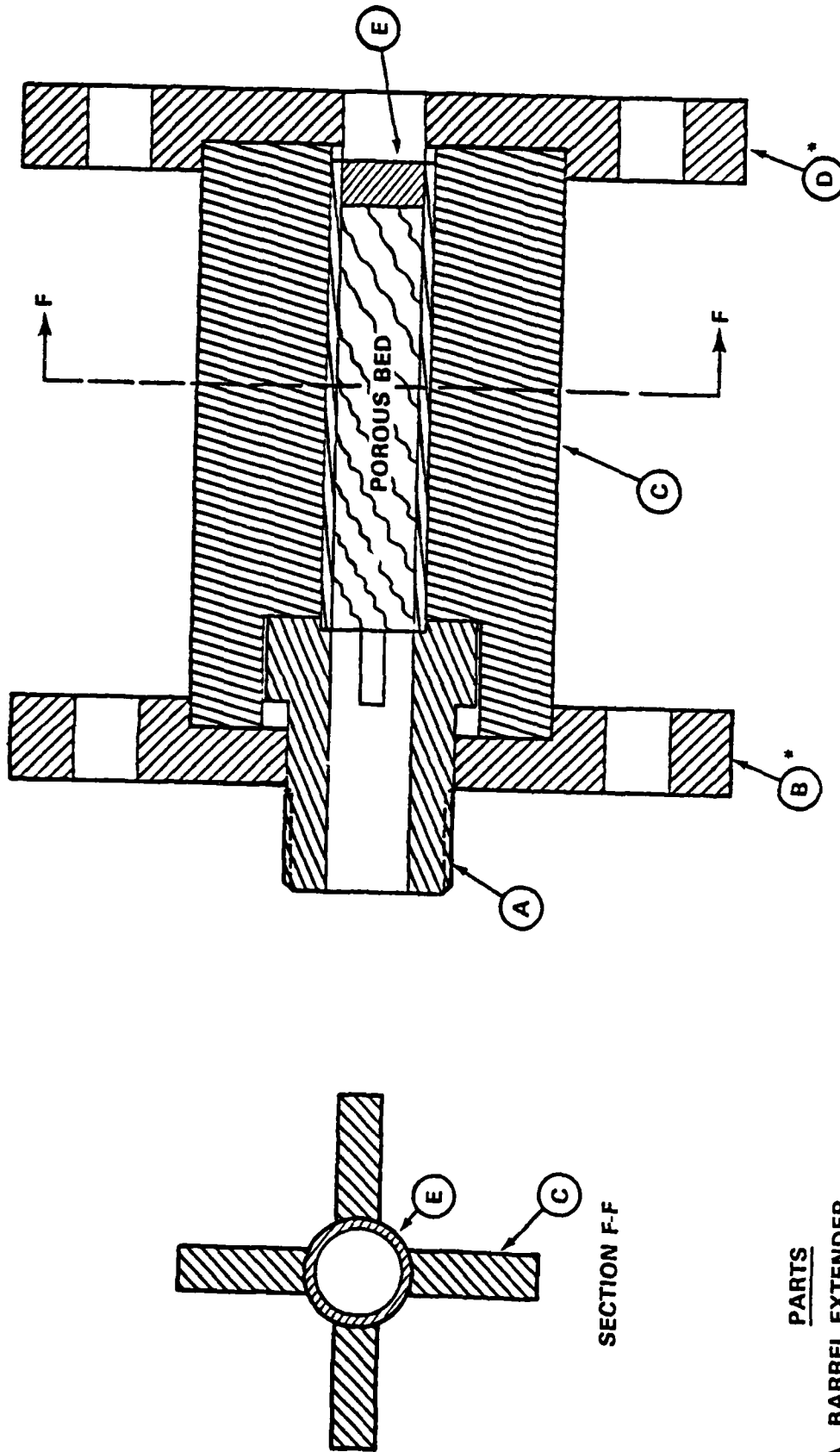
FIGURE 4. SCHEMATIC OF MODIFIED APPARATUS FOR PISTON DRIVEN COMPACTION

ignition and reaction buildup. However, the expansion of the Lexan tubes required a correction to the compaction data that was significant for higher stresses. In order to circumvent uncertainty of the correction, an apparatus was designed which increased bed confinement while still permitting flash radiography of the core of the porous bed. A schematic of this intermediate confinement arrangement in Figure 5 shows the porous bed in a thin (3.2 mm) wall aluminum tube that is supported (note Section F-F) along approximately half of its outer wall by steel bars.

The PDC data are summarized in Table 3. The bed lengths varied from 120.6 to 146.1 mm. In all experiments, except Shots PDC-16 and 17, a transparent disk covered the driven end of the barrel to maintain bed integrity and to avoid the injection of hot compressed air into the bed by the piston. These disks were nominally 0.8 mm thick, except for those experiments involving PRXW-109(E), for which the disks were 12.7 mm thick and held in place with fast setting epoxy. This was necessary because the "spring-back" of the bed after loading would otherwise push the disk out of the confining tube and change the initial bed density.

The transparent disk technique for obtaining compaction data in Shots PDC-2, 3, 12, and 13 involved both 0.7-1.7 mm thick PMMA disks and 1.0 mm thick RTV-615 disks in each experiment. When photographing Shots PDC-2 and 3 with a framing camera, the RTV disks remained visible despite significant tube deformation, whereas the light transmission through the PMMA disks failed. However, even with the limited field of view of the streak camera, the PMMA disks were more visible than the RTV disks in Shot PDC-12, perhaps because the stiffer PMMA disks allowed less shifting of the WC 231 bed. (WC 231 particles, as well as the other propellant particles listed in this report, flow easily.) The streak images of both the PMMA and RTV disks ended once the disks began moving in Shot PDC-13. For the relatively mild piston impacts in Shots PDC-6, 9, and 20, clear streak images of the 0.7-1.7 mm thick PMMA disks were recorded for Shots PDC-6 and 9, but not in Shot PDC-20 once the disks began moving. As in Shot PDC-13, the transparent disk technique in several DDT experiments provided no data other than the arrival time of a strong compaction wave. In view of the incompatibility of the transparent disks with the typically stronger compaction waves in PDC as compared to CGC experiments, most PDC data were obtained by flash radiography.

The measurement of porous bed compaction via flash radiography is actually based on the displacement of small metallic tracers packed into the bed at 6.4 mm increments. They consisted of either tungsten wires (0.4 mm diameter by 12.5 or 22.9 mm long) or lead disks (6.4 mm diameter by 0.04 mm thick). In order for the lead disks to retain their position and shape, they were not used in beds with particles significantly larger than the thickness of the disks. Following the IDC experiments, the flash radiography system was expanded from two to four channels. Since each listing of compaction data in Table 3 is from the tracer displacement between sequential pairs of radiographic exposures, four radiographs will provide three sets of data. When more than one set of data was obtained for an experiment, the data are listed in Table 3 in the order of the radiographic exposures; that is, the first listing of data is for compaction near the driven end of the bed. For Shot PDC-20, both data gathering techniques



PARTS

- A. BARREL EXTENDER
- B. MUZZLE PLATE
- C. TUBE SUPPORT
- D. CLOSURE PLATE
- E. ALUMINUM TUBE (25.4mm I.D., 31.8mm O.D., 146mm LONG) WITH CLOSURE PLUG

* PLATES ARE CONNECTED BY FOUR 3/4-10 NC THREADED RODS (NOT SHOWN)

FIGURE 5. SCHEMATIC OF PDC TEST SECTION FOR INTERMEDIATE CONFINEMENT

TABLE 3. SUMMARY OF PISTON DRIVEN COMPACTION EXPERIMENTS

INITIAL CONDITIONS*					OBSERVATIONS*					CALCULATIONS*	
SHOT NO.	POROUS BED MATERIAL	%TMD ₀	SET-UP	v _p (mm/μs)	u (mm/μs)	U (mm/μs)	%TMD _c	%ε _{qs}	IGNITION	%TMD _n	p _n (MPa)
PDC-2	Teflon 7C	60.0	A, DISKS	~0.27	0.188	0.43	114.7	-	-	106.6	112
-6				0.07	0.062	0.195	89.0	0.12	-	88.0	16.8
-41A			C, X-RAY	~0.07	0.052	0.293	79.0	-	-	79.0	15.7
-17			B, X-RAY	0.122	0.096	0.384	86.2	-	-	86.6	37.8
-16			B, X-RAY	~0.17	0.153	0.495	93.5	-	-	94.0	77.5
-3	Melamine	65.0	A, DISKS	0.19	0.148	0.480	95.1	-	-	93.9	72.7
-41B			C, X-RAY	~0.17	0.157 0.155 0.140	0.539 0.534 0.498	92.8 92.1 91.0	-	-	91.7 91.5 90.4	86.6 84.7 71.4
-19				~0.07	0.062 0.060 0.052	0.346 0.324 0.267	69.8 70.3 71.2	-	-	70.1 70.7 71.5	20.5 18.6 13.3
-24	Fluid A	57.6	B, X-RAY	0.129	0.109 0.109 0.112	0.413 0.410 0.425	75.9 78.3 78.3	0.25	YES	78.2 78.4 78.2	42.9 42.6 45.3
-9	WC 231	49.4	A, DISKS	0.11	0.095	0.300	72.5	0.11	YES	72.3	23.2
-12				0.12	0.104	0.313	76.4	-	YES	74.0	26.5
-13	Tetryl	57.8	A, DISKS	0.19	0.149	0.380	97.3	-	YES	95.1	56.7
-21			B, X-RAY	0.073	0.055 0.058 0.052	0.300 0.304 0.280	89.1 89.6 90.0	0.11	-	89.4 90.2 89.6	23.0 24.6 20.3
-25	Class D HMX	73.0	B, X-RAY	0.102	0.076 0.079 0.081	0.359 0.347 0.364	91.3 93.6 94.4	0.17	YES	92.6 94.5 93.9	37.9 38.1 41.0
-54			C, X-RAY	0.116	0.080 0.079 0.078	0.393 0.382 0.369	91.9 91.9 92.4	-	-	91.8 92.3 92.7	43.7 42.1 40.0
-22			B, X-RAY	0.125	0.101	0.432	95.8	-	YES	95.2	62.1
-28				0.072	0.066 0.062 0.070	0.227 0.229 0.258	106.4 105.0 103.5	0.42	NO	105.7 104.3 101.8	19.8 18.2 20.6
-29	PBXW-108(E)	75.0	B, X-RAY	0.134	0.112 0.114 0.109	0.375 0.386 0.363	108.8 106.6 106.8	0.44	NO	106.9 106.4 107.2	49.1 51.4 46.2
-30				0.260	0.151 0.154 0.162	0.457 0.426 0.440	112.5 114.9 118.0	0.84	YES	112.0 117.4 118.7	80.6 76.6 83.2
-20			B, DISKS	0.075	0.062	0.269	100.7	0.16	NO	97.4	20.8
-20			B, X-RAY	0.075	0.061 0.057 0.057	0.276 0.247 0.238	98.7 97.1 98.1	0.16	NO	96.3 97.5 98.6	21.0 17.6 16.9
-23			B, X-RAY	0.128	0.102 0.109 0.108	0.364 0.348 0.336	100.6 106.2 109.6	0.46	NO	104.2 109.2 110.5	46.2 47.2 45.1
-26	PBXW-109(E)	75.0	B, X-RAY	0.177	0.117 0.137 0.146	0.404 0.418 0.424	103.8 108.4 112.8	0.74	YES	105.6 111.5 114.4	58.8 71.2 76.9
-31			B, X-RAY	0.283	0.175 0.169	0.477 0.449	115.6 119.4	1.06	YES	118.4 120.2	103.7 94.3
-42			C, X-RAY	0.28	0.159	0.602	102.1	-	YES	101.9	118.9

* SET-UP

Apparatus: A. Figure 3, B. Figure 4, C. Figure 5
 Instrumentation: DISKS Same as in CGC experiments
 X-RAY Flash radiography of tracers
 v_p = Piston velocity just prior to impact

* ε_{qs} = Quasi-steady strain in outer tube wall

See Table 2 or Nomenclature for undefined column headings.

were utilized; the transparent disk data for the driven end of the bed reasonably agree with the first set of flash radiographic data.

As an example of flash radiographic data, the displacement (Δx) of the lead disks in the four radiographs from Shot PDC-41B are plotted in Figure 6. For each radiograph, the location of the compaction front is determined by the intersection of a line through the various tracer displacements (least square fit analysis usually performed on the first six tracers behind the front) and the horizontal axis of the plot, which corresponds to no displacement of the bed. For one-dimensional analysis, the slope (s) of that line through the displaced x-ray tracers is related to the reduced separation between the tracers and, therefore, the bed density: $\%TMD_c = \%TMD_o / (1 + s)$. The values reported for $\%TMD_c$ in Table 3 are averaged for two adjacent radiographs, since U and u are determined from front and particle movement, respectively, between adjacent radiographs.

While conducting these experiments, it was realized that the compaction data at the higher stresses, relative to the stresses in the ignitor and gas driven compaction experiments, were affected by the limitations of Lexan tube confinement. Even without porous bed reaction, the stresses were high enough to cause significant tube expansion or even tube rupture. According to the framing camera record of the backlit apparatus in Shot PDC-2, the ~ 120 MPa stress in the Teflon 7C caused the inner wall of the Lexan tube to expand and to crack immediately behind the compaction front; the tube ruptured before the compaction front reached the far end. The slower piston velocity in Shot PDC-3 (with melamine) did not result in visible tube deformation, yet a comparison of the compaction data with quasi-static data (see Discussion) suggests significant expansion of the Lexan tube. A worse case for tube expansion is shown in Table 3 for two experiments with ~ 0.28 mm/ μ s piston impacts of 75% TMD PBXW-109(E); the apparent compacted density in Lexan tube Shot PDC-31 was 112.8% TMD versus the more reasonable value of 102.1% TMD in the increased confinement of Shot PDC-42. A scheme for correcting the Lexan tube compaction data is presented in the Discussion.

In previous IDC^{4,5} and some PDC experiments, strain gages (SGs) were circumferentially mounted on the Lexan tubes to measure pressures indirectly in the porous beds, since any direct measurement is both difficult and expensive. For the Lexan tubes utilized in the previous and present studies, the SG measurement of outer wall strain (ϵ) is proportional (92.7 MPa/ $\%\epsilon$) to the inner wall stress (p_w) up to the 28 MPa elastic limit of the inner wall.⁵ In Shot PDC-6 the SG signature from a compaction wave was obtained in order to aid interpretation of SG data from DDT and IDC experiments, where gas pressure is also involved. Although the SG in Shot PDC-6 began responding before the CF arrived at its location and then understated the rate of pressure rise for the compaction wave, the p_w after the passage of the compaction wave nearly equalled the calculated jump pressure.⁵ In many of the subsequent PDC experiments, SGs were mounted at the same 63.5 mm position as in Shot PDC-6. When obtained, the quasi-steady values of strain (ϵ_{qs}), following passage of the compaction wave, are reported in Table 3; conversion of ϵ to p_w is not shown since the elastic limit of the tube was often exceeded.

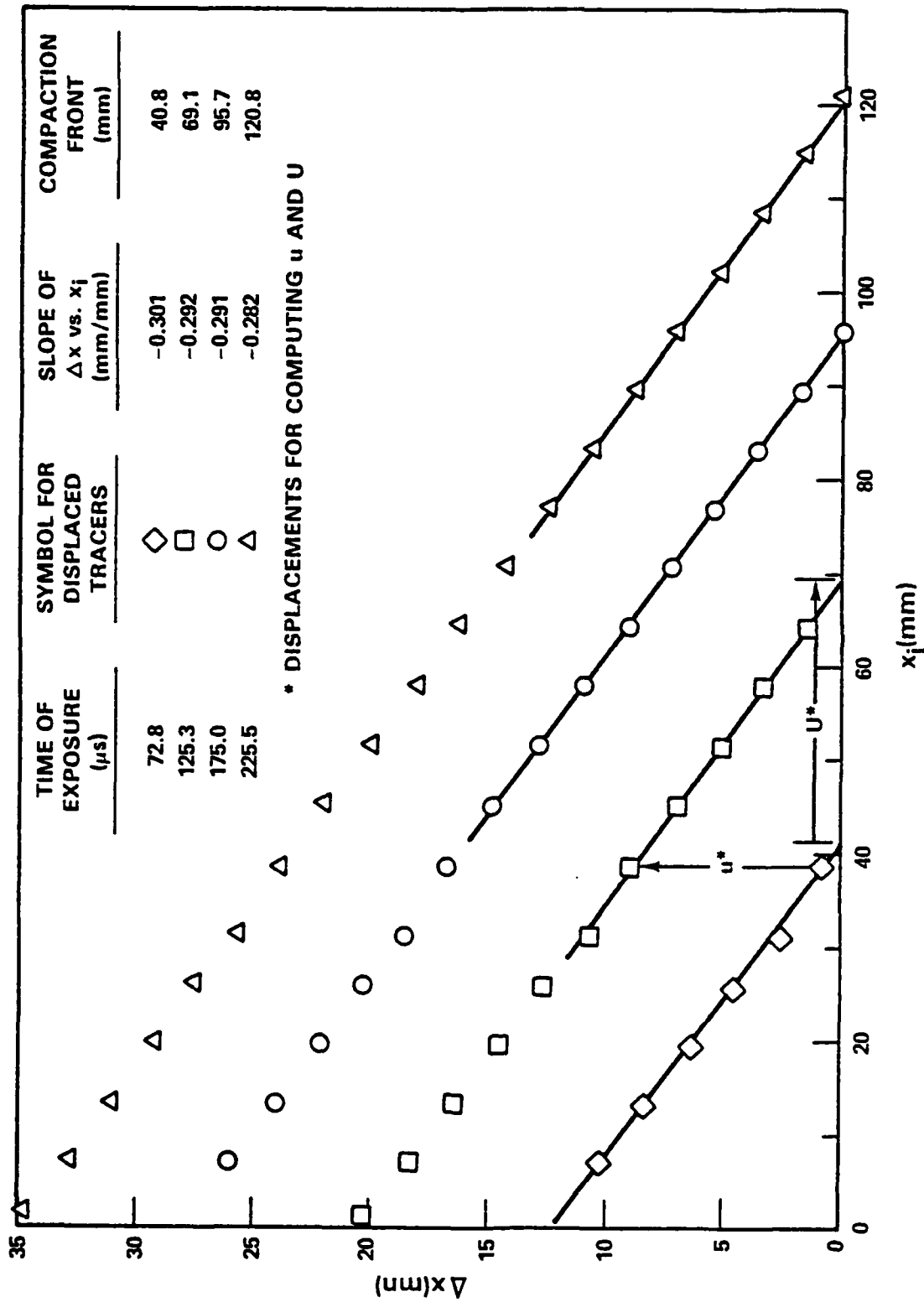


FIGURE 6. RADIOGRAPHIC DATA FROM SHOT PDC-41B: DISPLACEMENT OF TRACERS VERSUS THEIR ORIGINAL POSITION

As an example, plots of ϵ versus t are shown in Figure 7 for three HMX experiments. For the least energetic impact (Shot PDC-21) the SG responds much as in Shot PDC-6; that is, the SG responds before the CF reaches its location and then understates the rate of pressure rise. After 500 μ s there is a decline in ϵ followed by an increase that is associated with the rearward wave from reflection of the CF at the rigid far boundary, which is typical for nonreacting beds. In contrast, the fairly rapid increase in ϵ after 400 μ s for Shot PDC-25, a more energetic impact of the HMX, results from reaction. In Shot PDC-22, the most energetic impact of the HMX, the ϵ never becomes quasi-steady or reaches a plateau because of reaction. Thus the SG data were helpful in determining when reaction became significant enough to influence the compaction. Also, ϵ_{qs} will be used for correcting the compaction data for tube deformation.

For those experiments which exhibited compaction-initiated reaction (noted in Table 3), the listed compaction data are presumably not significantly affected by the reaction. In all cases, the data are from the vicinity of the compaction front (see Figure 6), whereas any growth of reaction first occurred at the driven end. Even then, compaction data are reported only if the growth of reaction did not significantly change the compaction parameters near the front. For example, the third set of Shot PDC-30 data in Table 3 shows slight increases in both u and U , probably from the slowly reacting explosive near the driven end of the bed. Aspects of the data related to reaction and its buildup are discussed in References 15 and 16 for several of the materials. Compaction-initiated reaction limits the stress (generally <100 MPa) which can be applied to porous energetic materials in order to obtain dynamic compaction data. Experiments on WC 231 and Class D HMX at piston velocities of 0.19 and 0.267 mm/ μ s, respectively, resulted in such prompt reaction that compaction data were not obtained.

RAMP LOADED COMPACTION EXPERIMENT

An apparatus was developed to compact a porous bed with a continuously increasing pressure pulse similar to that during DDT buildup. This ramp pressure generator was also designed for photographic recording by a synchronous camera in order to take advantage of the excellent images obtained with the Jacobs framing camera.¹⁹ Synchronization was possible because detonation product gases were used to accelerate a Teflon plug into the porous bed. The rate of formation of the detonation product gases and their confinement was controlled in such a way as to avoid shock wave damage of the porous bed confinement and disruption of the optical system.

The apparatus shown in Figure 8 was successfully used to ramp load a porous bed of Teflon 7C. The driver section contains an explosive helix in a well-confined free volume of about 40 cm³ that is separated from the test section by a Teflon plug. The explosive helix, consisting of a strip of explosive wound into a helical groove in a Lexan support rod, provides a gentle push for the plug by spreading the formation of detonation products over a time period of about 80 μ s. Inserting the explosive into the groove (2.5 mm wide x 2.5 mm deep x ~157 mm long) prevents detonation product gases from breaking the explosive strip and thereby terminating the propagation of detonation at the next helical turn. The use of a Lexan rod sufficiently isolates the helical

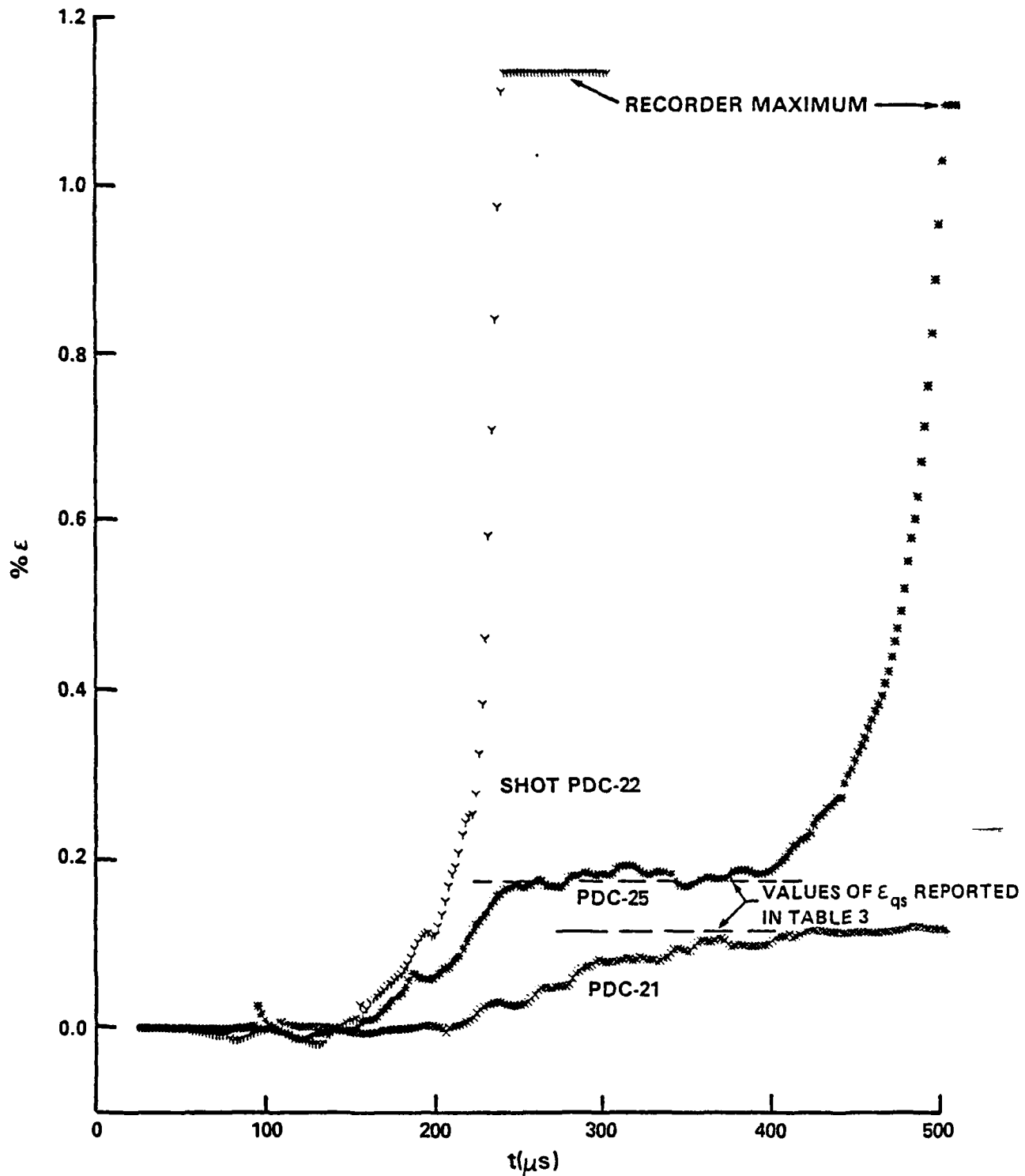


FIGURE 7. PERCENT STRAIN OF LEXAN TUBE CIRCUMFERENCE AT 63.5 mm VERSUS TIME DURING COMPACTION OF CLASS D HMX

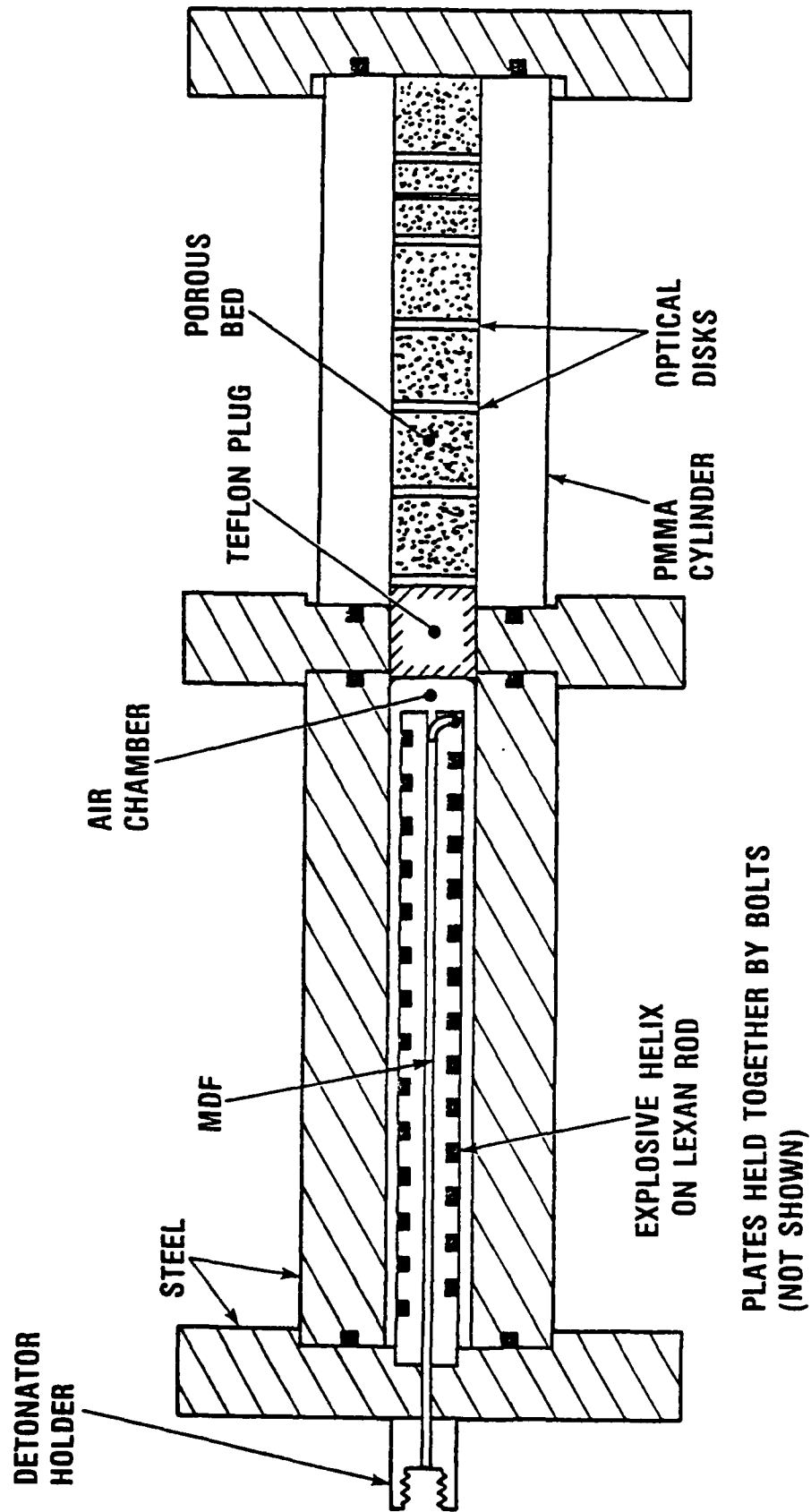


FIGURE 8. RAMP PRESSURE GENERATOR USED TO COMPACT TEFLON 7C POWDER

turns from damage by shock waves in the rod. Of the two explosives used, PBXN-301 and Detasheet, the PBXN-301 was more reliable for supporting detonation along the helix. As shown in Figure 8, the explosive is initiated by 2.5 gr/ft, mild detonating fuse (MDF) that is inserted into an axial hole extending from the detonator holder to the end of the support rod. The latter is designed with a radial slot so the MDF can bend and contact the explosive in the helix. The MDF was initiated by an exploding bridgewire detonator.

During preliminary tests of the ramp pressure generator, the motion of the 25.4 mm diameter Teflon plug was observed as it was propelled into air, without the test section attached, in order to characterize the driver system. The two tests involving the final configuration shown in Figure 8 had different explosive weight to volume ratios. The first test, Shot JK-052, had a driver section volume of 41.3 cm³, including the explosive. The weight of the PBXN-301 was 5.90 g (4.72 g PETN + 1.18 g inert), which represents an explosive weight to volume ratio (w/v) of 0.114 g/cm³. This loading corresponds to a closed bomb pressure of 152 MPa, which was not expected to be realized but is useful for comparison with other driver loadings. The Teflon plug, weighing 29.4 g, reached a maximum and fairly constant acceleration of 9.09×10^{-5} cm/ μ s² in 30-40 μ s, corresponding to a pressure of 53 MPa. In the next test, Shot JK-053, the volume of the driver section was reduced to 27.2 cm³, in order to increase the maximum pressure. This was accomplished by inserting a 146 mm long cylinder, consisting of ten turns of 0.13 mm thick Mylar film, against the inner wall of the chamber. The weight of PBXN-301 was 5.27 g (4.22 g of PETN), slightly less than in the previous test due to differences in loading technique. The resulting w/v of 0.155 g/cm³ corresponds to a closed bomb pressure of 207 MPa. A maximum acceleration of 1.014×10^{-4} cm/ μ s² for the Teflon plug was reached with no detectable delay, corresponding to a pressure of 61 MPa. The nearly constant pressure in both tests is the result of a constant ratio between the amount of reacting explosive and the immediate volume encompassed as the detonation travels along the helix.

In Shot JK-054, the complete system shown in Figure 8 was used with Teflon 7C powder packed to a density of 1.386 g/cm³ or 60.1% TMD. The weight of PBXN-301 in the driver section was 6.00 g (4.80 g of PETN). The w/v ratio of 0.116 g/cm³ corresponds to a closed bomb pressure of 155 MPa. Transparent disks of PMMA (2.2 mm thick) were placed at 25.4 mm intervals within the thick-walled (25.4 mm inner diameter) PMMA cylinder, starting at the Teflon plug. The last interval, however, was only 14.9 mm. A 0.75 mm PMMA disk was placed in the next to last interval, about halfway between the 2.2 mm disks, to see if thinner disks could be used with this technique. Light was supplied by exploding a 152 mm long, 0.05 mm diameter tungsten wire within a 1.5 mm bore capillary tube, that was located 150 mm behind the rear surface of the PMMA cylinder and parallel to its axis. The energy came from the discharge of a 56 μ F capacitor charged to 5 kV.

Position-versus-time plots of all seven optical disks are shown in Figure 9. Ramp loading on the end of the bed occurs over a time interval of 200 μ s according to the increasing velocity of the first disk. After that, the steady 0.114 mm/ μ s particle velocity of the disk indicates constant pressure on the end of the bed. Since the compressive waves from the top of the ramp travel

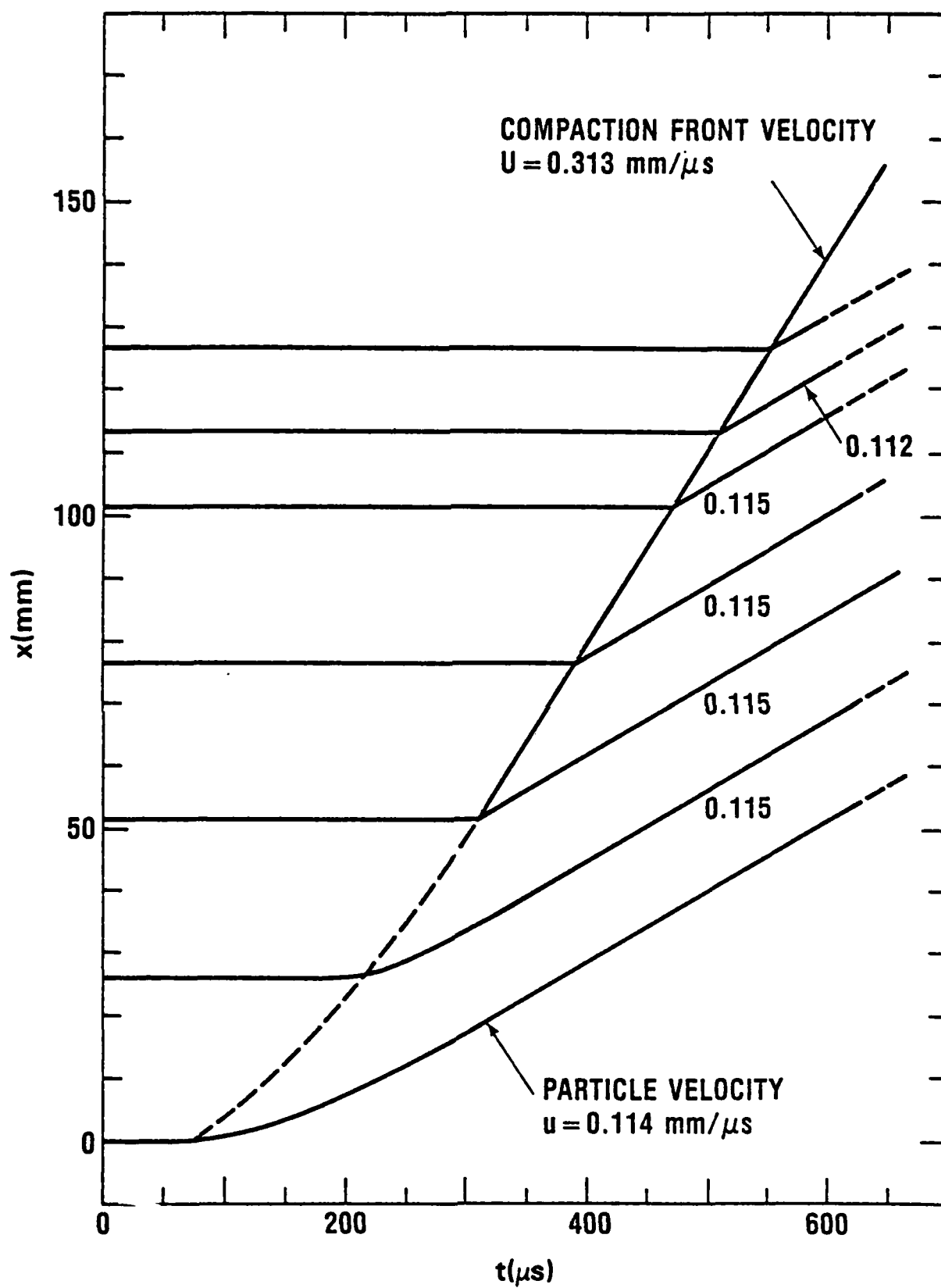


FIGURE 9. DISTANCE-TIME TRACES OBTAINED FROM PMMA OPTICAL DISKS IN 60.1% TMD TEFLON 7C USING THE RAMP PRESSURE GENERATOR, SHOT JK-054

faster than the initial waves, the ramp tends to steepen with time. Thus, the porous bed adjacent to the second disk is ramp loaded for only 50 μ s. By the time the wave front reaches the third disk at 50 mm, the abrupt increase in disk velocity indicates the end of any ramp loading. The dashed line in Figure 9 demarcates the approximate buildup of compaction front velocity. Following the ramp loading, there is a steady particle velocity of 0.112-0.115 mm/ μ s and a steady compaction front velocity of 0.313 mm/ μ s as the now abrupt compaction front (as in a PDC experiment) propagates to the far end of the bed. The reduced separation between disks indicates compression of the Teflon 7C to 95.3% TMD, which is in good agreement with the jump condition calculation (using $u = 0.114$ mm/ μ s) of $\%TMD_h = 94.6$. A calculated jump pressure of 49.6 MPa is nearly identical to the maximum 53 MPa pressure which accelerated the unrestrained Teflon plug in Shot JK-052.

SHOCK DRIVEN COMPACTION EXPERIMENTS

In two experiments, an explosively driven shock wave was used to compact the porous bed. The schematic of the apparatus in Figure 10 uses the shock wave originating from a NOL Large Scale Gap Test donor/attenuation system, with the diameter of the donor end of the gap reduced in order to fit into the confining tube. Assuming no effect from this modification, the peak pressure at the end of the 71.1 mm long gap would be 1.01 GPa. The loading of the PMMA tube and the recording of the compaction process are essentially the same as in the previously discussed ramp loaded experiment.

The first experiment, Shot JK-048, involved coarse-grain sucrose of random particle size packed to a density of 1.0 g/cm³ (63.0% TMD) in a 102 mm long tube. A 2 mm thick disk of RTV 615 was located between each of the four 20 mm increments of sucrose and on each end of the bed. The distance-time traces for the disks in Figure 11 show the particle and compaction front velocities decreasing with time. Changing disk separations, caused by the significantly varying particle velocities, did not permit a direct measurement of compaction; however, both compaction and pressure from jump condition calculations ($p_0 = 0$) are listed below for each disk. Surprisingly, compaction appears to be a weak function of pressure.

Disk No.	u (mm/ μ s)	U (mm/ μ s)	$\%TMD_h$	p_h (MPa)
1	0.107	0.54	78.5	57.8
2	0.089	0.45	78.5	40.1
3	0.069	0.39	76.5	26.9
4	0.064	0.35	77.1	22.4

For the next experiment, Shot JK-056, a porous bed of 60% TMD Teflon 7C was selected in order to compare compaction data with Teflon 7C data from other arrangements. To investigate the possibility that the RTV disk/wall friction was significant in the previous experiment, transparent disks of PMMA were used.

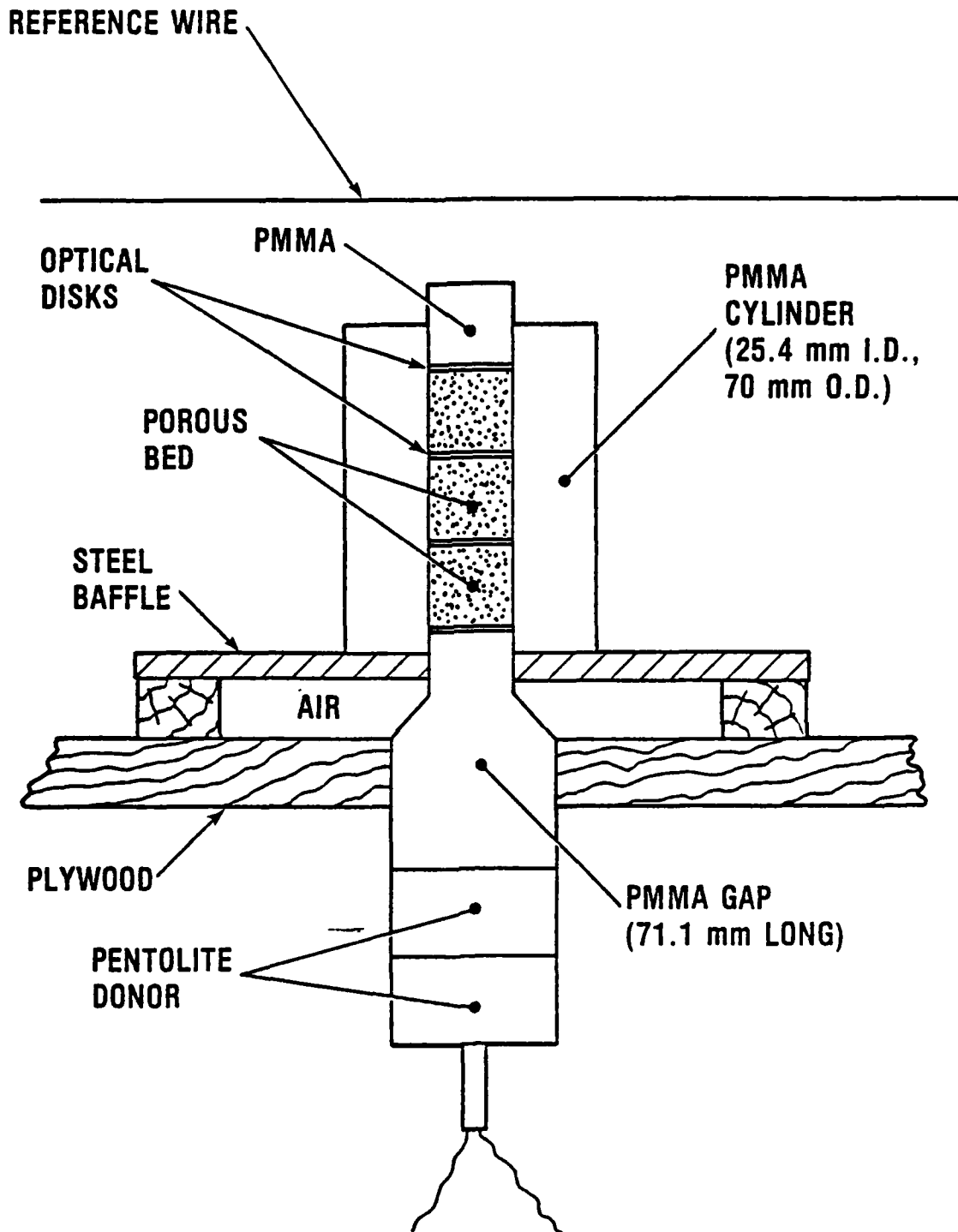


FIGURE 10. GAP TEST ARRANGEMENT USED TO RECORD PARTICLE MOTION IN POROUS MATERIAL BY LIGHT TRANSMITTED THROUGH OPTICAL DISKS

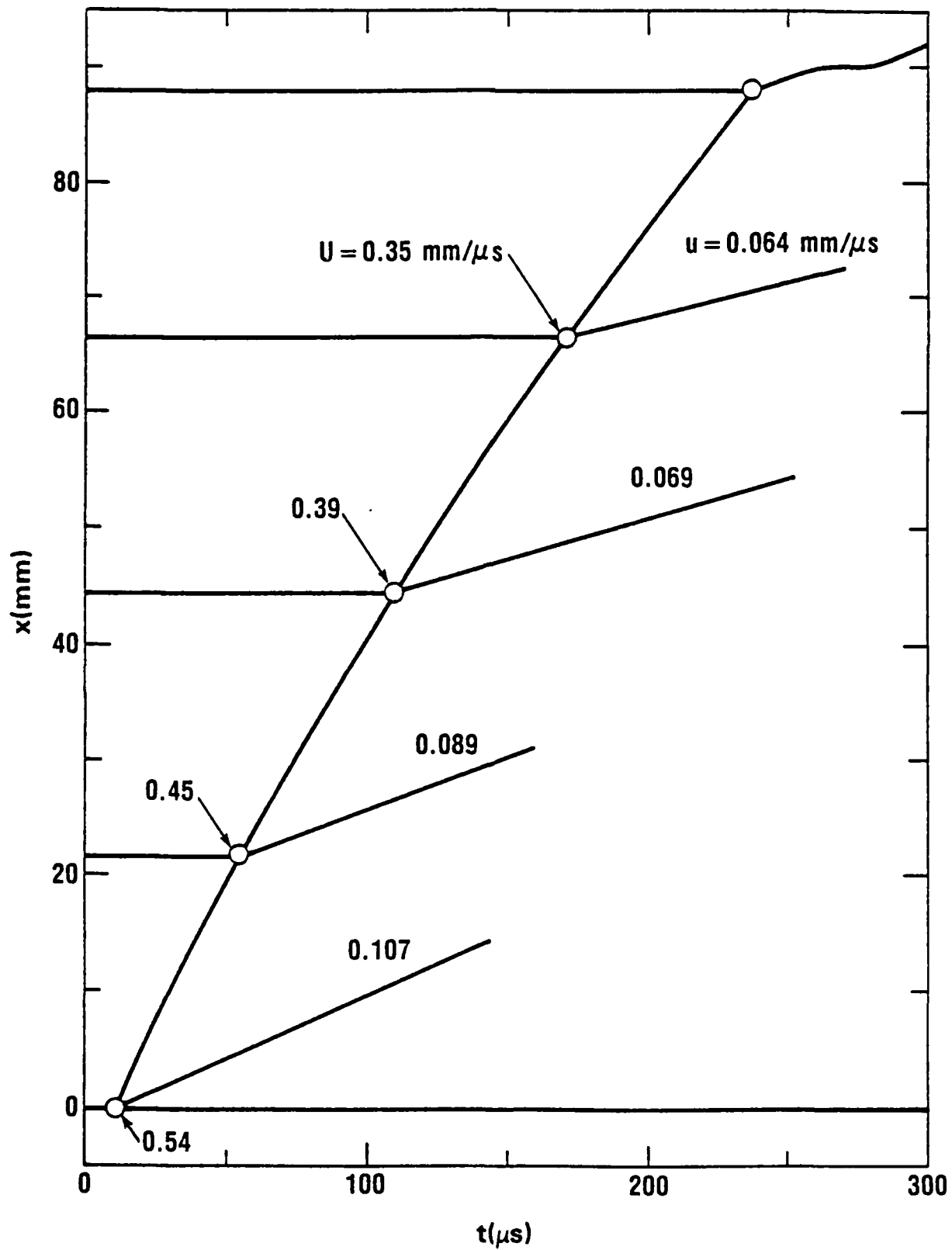


FIGURE 11. DISTANCE-TIME TRACES OBTAINED FROM RTV OPTICAL DISKS IN LOW DENSITY SUCROSE USING GAP TEST ARRANGEMENT, SHOT JK-048

The 149 mm long confining tube was packed with five 24.65 mm increments of Teflon 7C, with 0.75 mm thick disks separating each increment and on each end of the bed. The 15 mm space beyond the last transparent disk was filled with low density Teflon 7C, which projected about 0.5 mm above the end of the PMMA tube.

The distance-time traces shown in Figure 12 for Shot JK-056 were disappointing because of the early failure of the light transmission through the test section. Only the first disk moved a reasonable distance, with a velocity of 0.0993 mm/ μ s, before the light transmission ended; the second disk had just started to move, and subsequent disks had not moved yet. The initial motion of the first two disks indicates a compaction front velocity of 0.267 mm/ μ s. Jump condition calculations yield $\%TMD_h = 95.5$ and $p_h = 36.8$ MPa.

The failure of the light in Shot JK-056 was probably caused by detonation products spanning the gap and impacting the bottom of the tube. The far end of the tube had begun to move 90 μ s after the initial motion of the first disk, whereas there was no motion observed for the final (sixth) disk even after 500 μ s. Apparently, the PMMA tube was both set into motion and expanded, so that it could slide over the core of Teflon 7C without setting it into motion. When the compaction process reached each disk position, the expanded tube would permit some Teflon 7C to flow around the edges of the disk, thus blocking the light.

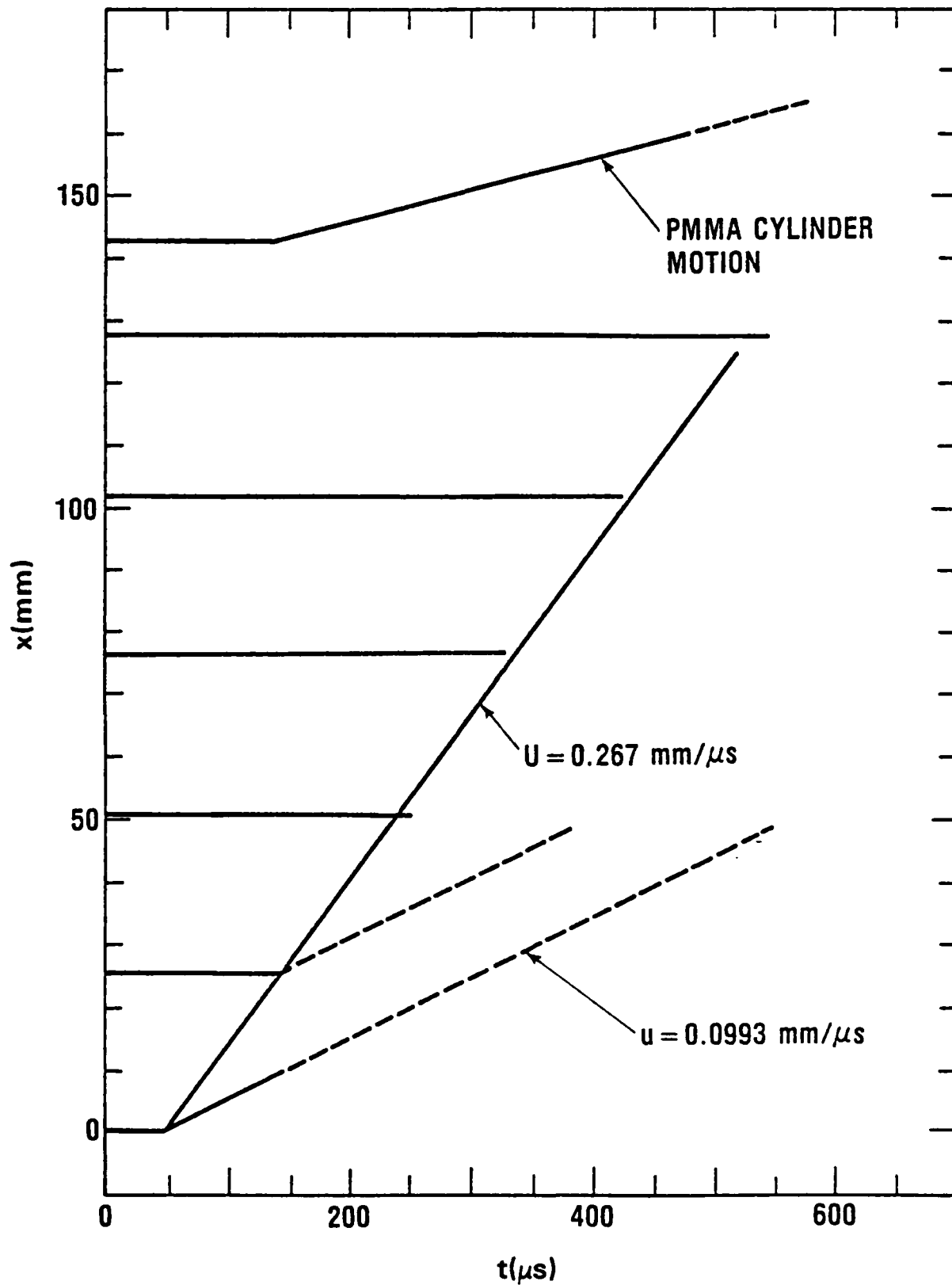


FIGURE 12. DISTANCE-TIME TRACES OBTAINED FROM PMMA OPTICAL DISKS IN 60% TMD TEFLON 7C USING GAP TEST ARRANGEMENT, SHOT JK-056

CHAPTER 3

DISCUSSION

Materials that were compacted fall into two distinct groups: PBXs, which were essentially compacted to TMD at the lowest pressures of interest, and non-PBXs, which still contained porosity at the highest experimental pressures. For most of the non-PBXs there are quasi-static measurements for comparison with the dynamic data, whereas comparable measurements were not conducted for the PBXs. Therefore, the data for the two groups of materials will be analyzed and discussed separately.

The dynamic data for the non-PBXs are summarized in Table 4, along with suggested corrections for data obtained in the low confinement of Lexan tubes. To be consistent with Elban's reporting of quasi-static measurements, the porous bed pressure (p_h) is converted to the average solid stress:

$$\tau_i = \begin{cases} 100 p_h / \%TMD_h, & \%TMD_h < 100 \\ p_h & , \%TMD_h \geq 100 \end{cases} \quad (3)$$

For compaction pressures >40 MPa, deformation of a Lexan tube is large enough to require correction of compaction data obtained from axial displacement of x-ray tracers or transparent disks. Even a small increase in tube diameter, if unaccounted for, results in a significant increase in axial compaction. The corrected (one-dimensional) data are useful for comparison with the quasi-static data obtained in a hardened steel mold and the observations of dynamic compaction during DDT in a steel tube arrangement. Presumably there was significant deforming of the three PMMA tubes that were used, but no correction to the data was attempted because of their limited use and the absence of strain gage measurements. Corrections to the Lexan tube data assumed that the bed diameter in the compacted region (d) had increased uniformly from its original diameter ($d_o = 25.4$ mm). Equations (1) and (2) for the jump condition can be approximately modified to account for tube expansion by the additional terms shown in parentheses:

$$\%TMD = \frac{\%TMD_o U}{U-u} \left(\frac{d_o}{d} \right)^2, \quad (4)$$

$$p = p_o + \frac{\%TMD_o}{100} TMD U u \left(\frac{2d_o^2}{d^2 + d_o^2} \right). \quad (5)$$

TABLE 4. SUMMARY OF NON-PBX COMPACTION DATA WITH SUGGESTED CORRECTIONS FOR LEXAN TUBE EXPANSION

POROUS BED MATERIAL	SHOT NO.*	UNCORRECTED DATA			CORRECTED DATA†			
		%TMD _h	P _h (MPa)	τ_i (MPa)	(P _w = P _h) %TMD τ_i	(P _w = ϵ_{qs}) %TMD τ_i		
MELAMINE	PDC-41A	79.0	15.7	19.8	-	-		
	-17	86.6	37.8	43.6	82.3	44.7		
	-16	94.0	77.5	82.4	84.7	86.7		
	-3	93.9	72.7	77.4	85.1	81.2		
	-41B	91.7	86.6	94.4				
		91.5	84.7	92.5	-	-		
		90.4	71.4	78.9				
TEFLON 7C	S-79 ¹	80.7	9.2	11.4	79.7	11.4	79.6	11.4
	CGC-6	78.4	8.6	11.0	77.5	11.1	-	-
	-9	82.1	12.4	15.1	80.7	15.3	-	-
	-10	85.0	10.5	12.4	83.7	12.5	-	-
	PDC-6	88.0	16.8	19.1	86.0	19.3	86.6	19.3
	JK-054 ²	94.6	49.6	52.4	-	-	-	-
	-056 ³	95.5	36.8	38.5	-	-	-	-
SUCROSE	JK-048 ³	78.5	57.9	73.7				
		78.5	40.2	51.1				
		76.5	27.0	35.3				
		77.1	22.5	29.2				
WC 140	CGC-12	65.1	11.4	17.5	64.1	17.6		
	-13	67.3	22.9	34.0	65.2	34.5		
	-14	67.6	17.9	26.5	66.0	26.8		
FLUID A	CGC-18	66.8	6.3	9.5	66.2	9.5	-	-
	-19	67.3	10.3	15.4	66.4	15.5	-	-
	PDC-19	70.1	20.5	29.2	68.2	29.6		
		70.7	18.6	26.3	68.9	26.6	-	-
		71.5	13.3	18.6	70.2	18.8		
	PDC-24	78.2	42.9	54.8	73.8	56.4	75.8	55.7
		78.4	42.6	54.3	74.0	55.8	76.0	55.1
		78.2	45.3	58.0	73.5	59.8	75.7	58.9
TS 3660	CGC-16	63.6	10.5	16.5	62.6	16.6		
	-17	66.7	17.5	26.3	65.0	26.6		
WC 231	CGC-22	72.1	19.4	26.9	70.2	27.3	-	-
	-23	69.6	14.9	21.5	68.2	21.7	-	-
	PDC-9	72.3	23.2	32.1	70.0	32.6	71.3	32.3
	-12	74.0	26.5	35.8	71.3	36.4	-	-
TETRYL	PDC-13	95.1	56.7	59.7	88.0	62.0		
CLASS D MMX	PDC-21	89.4	23.0	25.7	86.6	26.1	88.1	25.9
		90.2	24.6	27.2	87.2	27.7	88.9	27.4
		89.6	20.3	22.6	87.2	23.0	88.4	22.8
	PDC-25	92.6	37.9	41.0	87.9	42.0	90.6	41.4
		94.5	38.1	40.3	89.7	41.4	92.5	40.8
		93.9	41.0	43.7	88.8	44.9	91.9	44.1
	PDC-54	91.8	43.7	47.7				
		92.3	42.1	45.6	-	-	-	-
		92.7	40.0	43.2				
	PDC-22	95.2	62.1	65.2	87.5	68.0	-	-

* SHOT NO. identifies the experimental arrangement except as noted:

1. IDC, 2. RLC, 3. SDC

† Data corrections for beds packed in Lexan tubes

Evaluation of those terms in parentheses indicates that the correction has more influence on the extent of compaction than on compaction pressure.

The values for d were arrived at in two ways. Both methods assume elastic strain and plane stress in a thick-walled cylinder, although the inner wall region undergoes plastic deformation in the pressure range of interest. The equations used for both methods can be derived from the equations in Appendix A of Reference 20. One method assumes isotropic pressure in the compacted region; that is, the pressure on the inner wall (p_w) is the same as the calculated jump condition pressure (p_h). In this case,

$$d = \frac{[(1 - \nu)d_o^2 + (1 + \nu)d_e^2]p_h}{E_y d_o [(d_e/d_o)^2 - 1]}, \quad (6)$$

where $\nu = 0.4$ is Poissons ratio, $d_e = 76$ mm is the outer diameter of the cylinder, and $E_y = 2.38 \times 10^5$ MPa is Young's modulus of elasticity for Lexan. The other method determines d from strain gage measurements of tangential strain (ϵ_{qs}) at the outer tube wall:

$$d = [(1 - \nu)d_o^2 + (1 + \nu)d_e^2] \epsilon_{qs} / 2 d_o, \quad (7)$$

where values for ϵ_{qs} are listed in Table 3.

The magnitude of the corrections for data obtained in Lexan tubes is demonstrated in Figure 13a, where the dynamic data in Table 4 for melamine are plotted with Elban's quasi-static data. The corrections primarily affect the extent of compaction, those corrections becoming large at the higher stresses (~9% TMD at 80 MPa). Without accounting for tube expansion, the melamine appears easier to compact dynamically than quasi-statically, which is contrary to expectation. When tube expansion is considered by assuming $p_w = p_h$, the results suggest that melamine is much more difficult to compact dynamically. The actual dynamic data, however, are most likely represented by the intermediate confinement results. Those results closely agree with the quasi-static data, and, therefore, indicate little strain rate dependence. The over-correction of the Lexan tube measurements results from p_w not being as great as p_h . According to measurements of tube strain during other experiments, $p_w = 1/2 p_h$ for Fluid A and HMX whereas $p_w = p_h$ for Teflon 7C and the PBXs. Melamine apparently behaved like Fluid A and HMX, and the assumption that $p_w = p_h$ is an upper limit to the correction of the Lexan tube measurements.

For sucrose and tetryl, quasi-static data are not available for comparison with the dynamic data. When plotted with the melamine data in Figure 13a, sucrose is shown to be more resistant to compaction. Actually, sucrose is even more difficult to compact than shown, since those measurements are not corrected for expansion of the PMMA tube which confined the bed. The single data point for tetryl is not plotted because of the uncertainty in the rather large correction for Lexan tube expansion.

Teflon 7C was compacted by all techniques discussed in this report, and in the earlier IDC experiments. Despite the scatter in the plotted data in Figure 13b, there is no indication that the dynamic data were significantly influenced by the various compaction techniques. The plotted data from Lexan

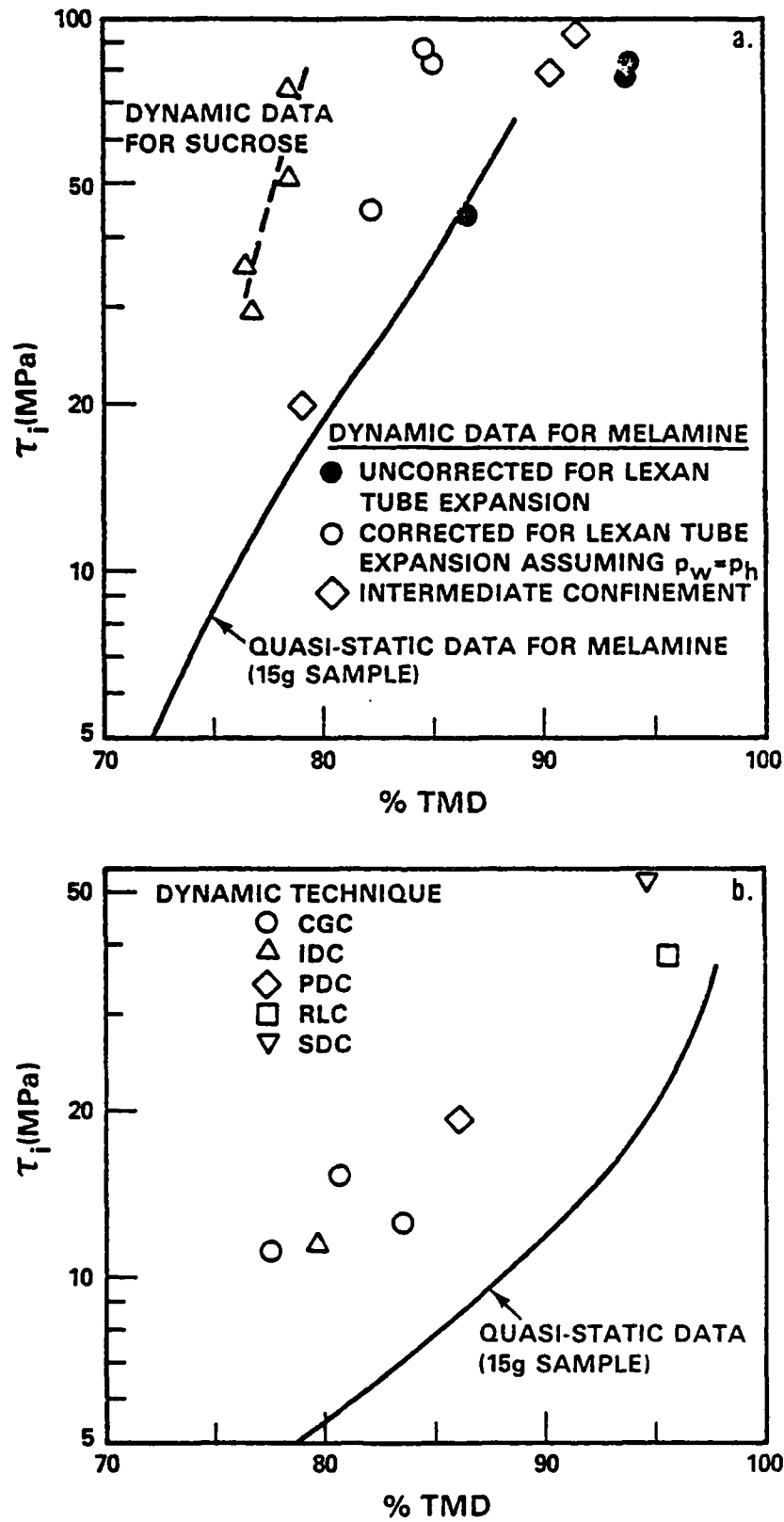


FIGURE 13. COMPACTION DATA FOR INERT MATERIALS.
A. MELAMINE AND SUCROSE, B. TEFLON 7C

tube experiments are corrected for tube expansion assuming $p_w = p_h$, which is reasonable according to two measurements of tube strain. In any case, the corrections are relatively small compared to those for the melamine experiments,⁷ since the stresses are much lower. When comparing the dynamic and quasi-static data in Figure 13b, it is observed that Teflon 7C is noticeably more difficult to compact dynamically. This is consistent with the compaction rate dependence for Teflon 7C that was modeled by Coyne and Elban.¹¹

The compaction data for the single- and double-base propellants are plotted in Figures 14a and 14b, respectively. When strain gage measurements were available, they were used in correcting the data. Otherwise, the corrections were made by assuming $p_w = p_h$. The dynamic data are in reasonable agreement with Elban's quasi-static data,⁹ except for WC 231. The apparent compaction rate sensitivity of WC 231, as well as its ease of compaction, may be due to the high nitroglycerin content and/or the rolling process that deformed the particles during manufacture (the other propellants were not rolled).

The dynamic and quasi-static^{10,12} data for Class D HMX are plotted in Figure 15. Since tube strain was not measured in Shot PDC-22, the plot shows both the uncorrected datum and the rather large correction to that datum, based on assuming $p_w = p_h$. Measurements of tube strain in Shots PDC-21 and 25 indicate that $p_w \approx 1/2 p_h$; the corrected compaction data based on these results and the intermediate confinement data for Shot PDC-54 seem to follow the same compaction curve. The dynamic data fall within the observed range of the quasi-static measurements. That range is much larger than for other materials, which may be caused by density variations within each sample. The existence of those variations is consistent with the large differences in %TMD between the beds packed for quasi-static and dynamic compaction. Both arrangements employed 25.4 mm diameter beds and used HMX from the same container. Each quasi-static experiment involved a single 15 g increment, compressed to 65% TMD by the weight of the ram. Each dynamic experiment had many 4.5 g increments that were at ~72% TMD just from pouring them into the tube before hand pressing them to 73.0% TMD for consistency. The incremental introduction of small amounts of HMX resulted in a tighter and probably more uniform packing of the crystals, which possibly affected subsequent compaction. Although a comparison of the dynamic and quasi-static data does not permit an evaluation of rate effects, a separate study¹² suggests a small effect for coarse HMX compaction.

Dynamic data for PBXs are summarized in Table 5, along with suggested corrections for the data taken in the low confinement of Lexan tubes. Since the PBXs were always compacted to essentially TMD, it is more instructive to compare particle velocity, instead of extent of compaction, with pressure or stress. Also, since no comparison with quasi-static data is sought, p_h will not be converted to τ_i ; however, $p_h = \tau_i$ for %TMD_n > 100 (Equation 3). All Lexan tube experiments had strain gage measurements for correcting %TMD_n and p_h . However, the assumption that $p_w = p_h$ resulted in insignificant differences, indicating that the pressure behind the compaction fronts was isotropic. The

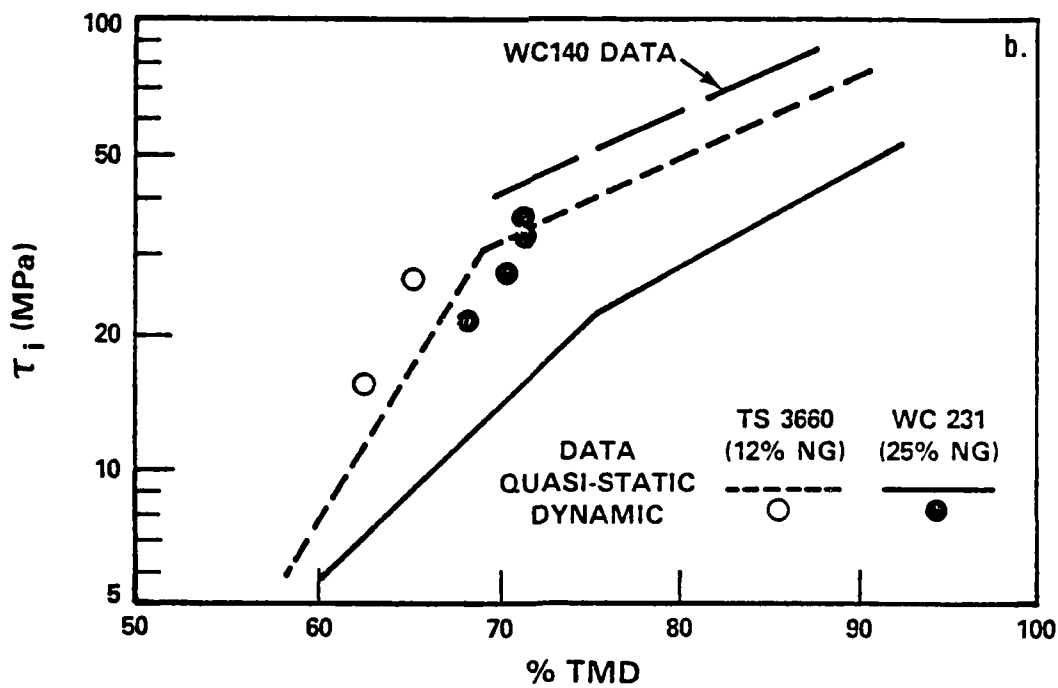
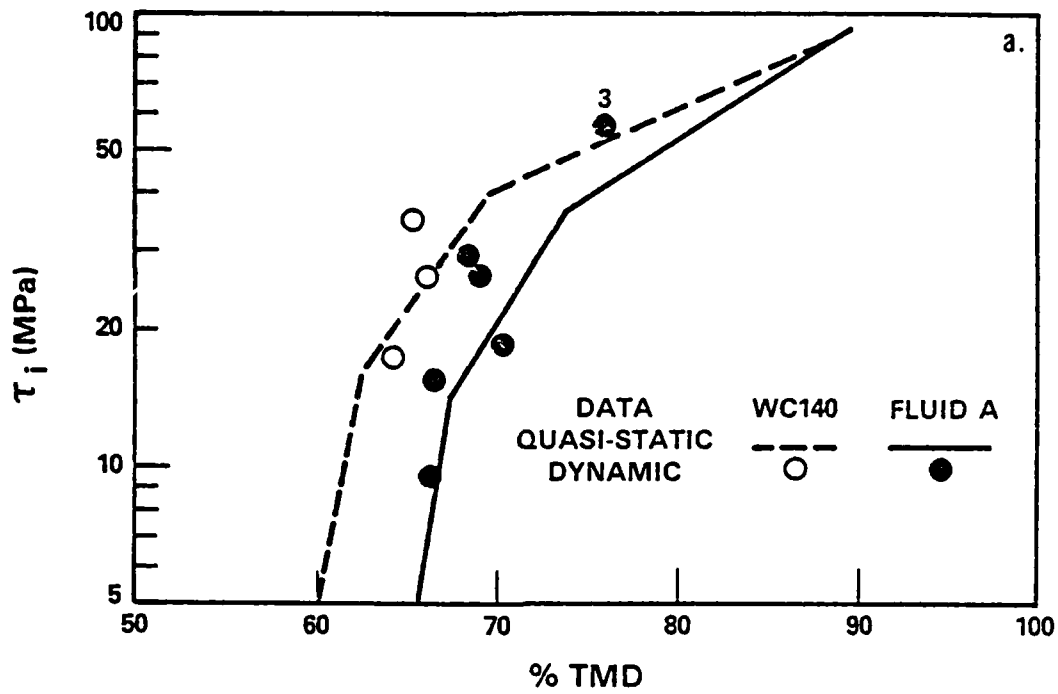


FIGURE 14. COMPACTION DATA FOR A. SINGLE-AND B. DOUBLE-BASE PROPELLANTS

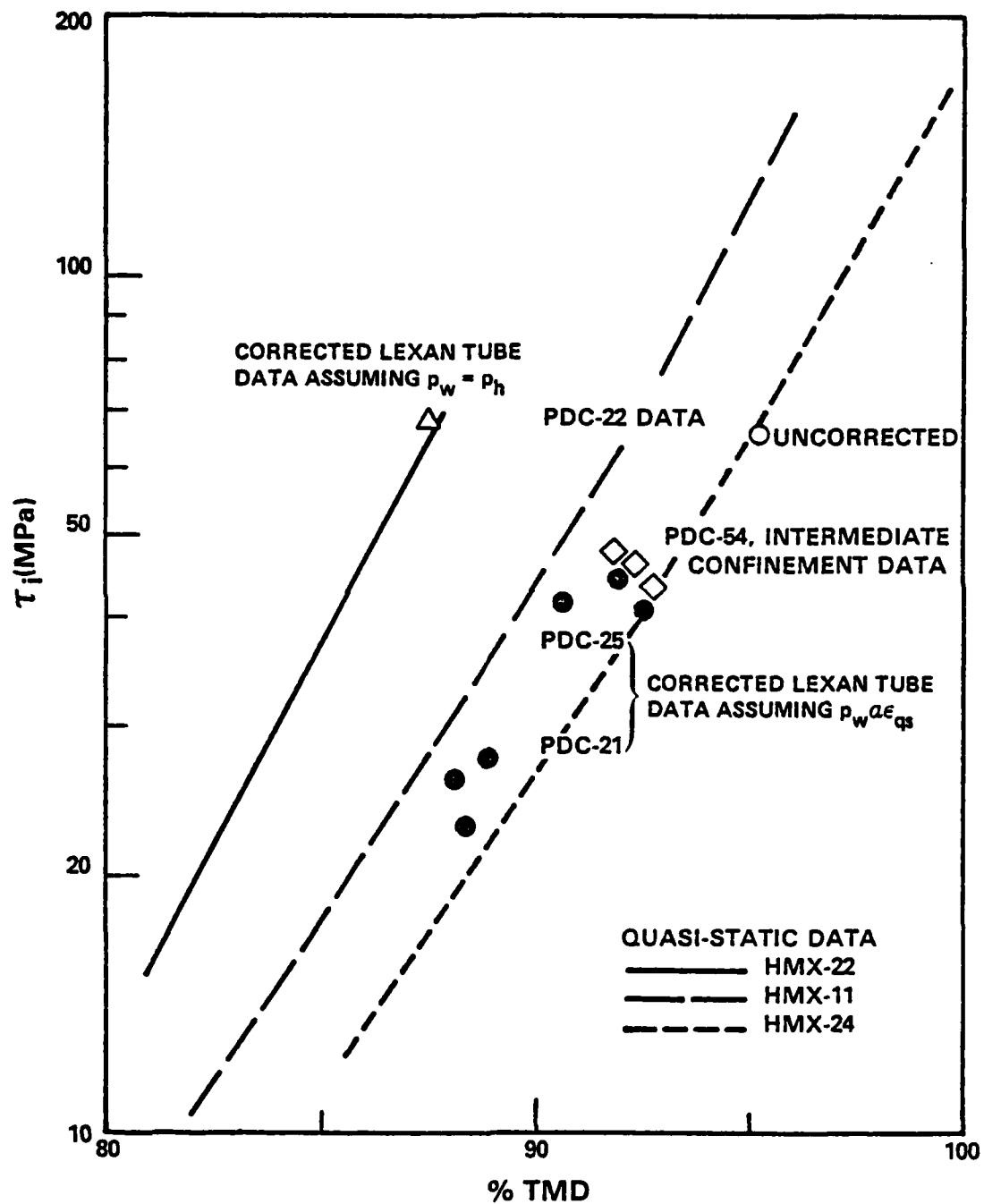


FIGURE 15. COMPACTION DATA FOR CLASS D HMX

TABLE 5. SUMMARY OF PBX COMPACTION DATA WITH SUGGESTED CORRECTIONS FOR LEXAN TUBE EXPANSION

POROUS BED MATERIAL	SHOT NO.	UNCORRECTED DATA*			CORRECTED DATA†		
		u (mm/μs)	%TMD _h	P _h (MPa)	u (mm/μs)	%TMD	p (MPa)
PBXW-108(E) %TMD ₀ = 75.0	PDC-28	0.070	105.7	19.8	0.064	100.2	19.1
		0.066	104.3	18.2	0.060	98.9	17.6
		0.068	101.8	20.6	0.062	96.5	19.9
	PDC-29	0.112	106.9	49.1	0.103	101.1	47.6
		0.114	106.4	51.4	0.104	100.6	49.9
		0.109	107.2	46.2	0.100	101.3	44.8
	PDC-30	0.151	112.0	80.6	0.129	100.8	76.2
		0.154	117.4	76.6	0.134	105.7	72.5
		0.162	113.7	83.2	0.142	106.8	78.7
PBXW-109(E) %TMD ₀ = 75.0	PDC-20	0.061	96.3	21.0	0.058	94.3	20.8
		0.057	97.5	17.6	0.055	95.5	17.4
		0.057	98.6	16.9	0.055	96.6	16.8
	PDC-23	0.102	104.2	46.2	0.092	98.3	44.8
		0.109	109.2	47.2	0.100	103.0	45.8
		0.108	110.5	45.1	0.099	104.2	43.8
	PDC-26	0.117	105.6	58.8	0.100	96.2	56.0
		0.137	111.5	71.2	0.120	101.6	67.9
		0.146	114.4	76.9	0.129	104.2	73.4
	PDC-31	0.175	118.4	103.7	0.147	103.8	96.9
		0.169	120.2	94.3	0.143	105.4	88.1
	PDC-42	0.159	101.9	118.9	a		

*From Table 3

†Corrections based on strain gage measurements of Lexan tube experiments at intermediate confinement

corrected pressure and extent of compaction were then used to compute a corrected particle velocity with the equation

$$u = 100 \text{ TMD} (p - p_0) \left(\frac{1}{\%TMD_0} - \frac{1}{\%TMD} \right)^{1/2} \quad (8)$$

The correction for tube expansion results in a reduced value for the particle velocity, and, although not shown, the corrected compaction front velocity increases.

The deviation of the corrected values for $\%TMD_h$ (in Table 5) from TMD is an approximate measure of the accuracy of the corrected data. Although there is some bulk compression of the PRXs, especially at the higher pressures employed in this study, the errors from neglecting bulk compression are not greater than those associated with correcting for tube expansion. A bulk modulus of 4.81 GPa for PBXW-109(E) was computed from the equation $B = \rho(c_l^2 - 4/3 c_s^2)$, where c_l is the longitudinal velocity and c_s is the shear velocity. W. Elban has ultrasonically measured $c_l = 1.71 \text{ mm}/\mu\text{s}$ at a frequency of 0.5 MHz. W. Madigosky reports²¹ a shear modulus of 0.025 GPa for PBXW-109(E), based on ultrasonic measurements at a frequency of 2.2 KHz; the computed shear velocity of 0.12 mm/ μs is so low that it does not significantly influence the computation for B. For the highest pressure PBXW-109(E) experiment, Shot PDC-42, the bulk compression at 118.8 MPa would result in compaction to 102.5% TMD, if no porosity remained. The slightly lower $\%TMD_h = 101.9$, which is listed in Table 5, may indicate some porosity; however, the difference is small enough to be attributed to experimental error.

The corrected and uncorrected data for compaction of PBXW-108(E) and PBXW-109(E) are plotted in Figures 16a and 16b, respectively (corrected data from the lowest pressure experiment for each PRX are not shown, since the small corrections would confuse the plot). The solid line in each figure represents the reference for compaction to TMD and is obtained from the previous equation by using $\%TMD = 100$. Corrected data for both PBXs reasonably agree with the reference line, especially for the lower pressures where tube expansion is not as extensive. The one data point for intermediate confinement of PBXW-109(E) (Shot PDC-42) nearly falls on the reference line, the deviation probably due to bulk compression.

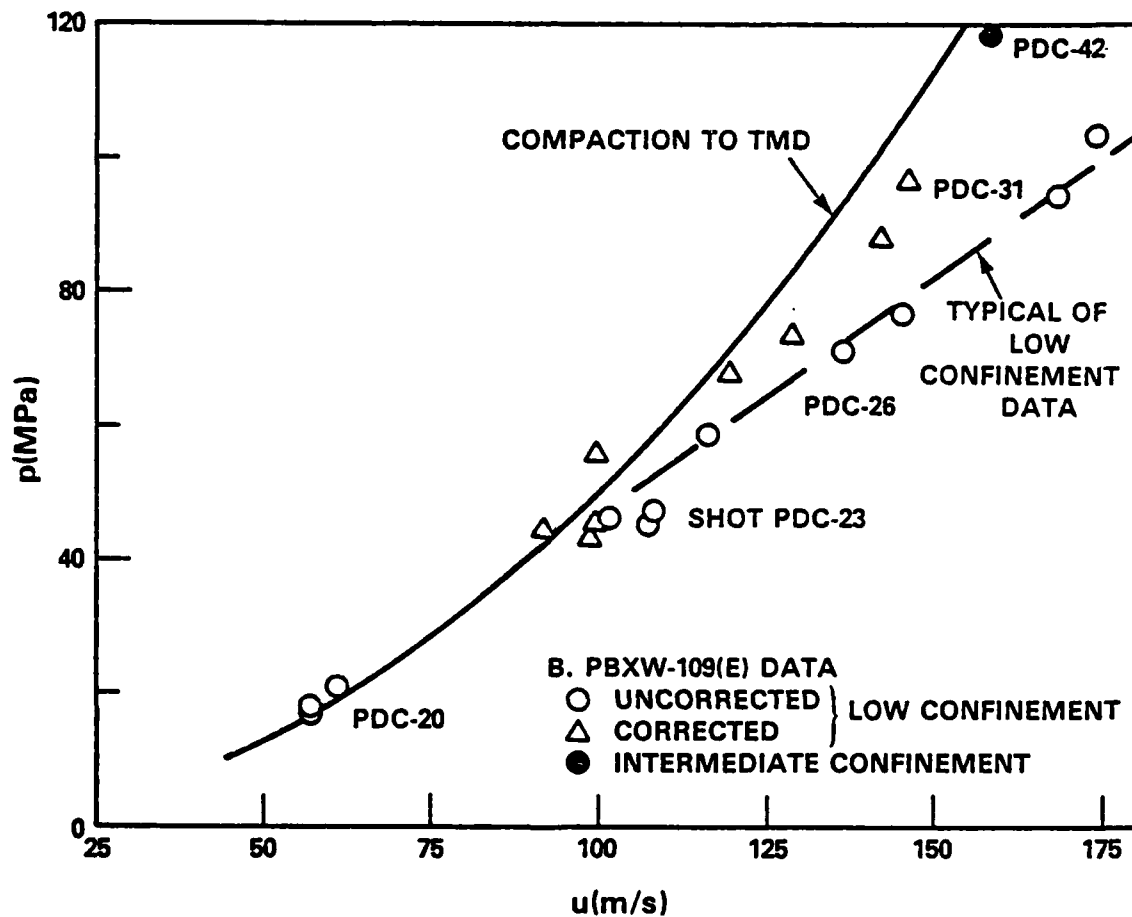
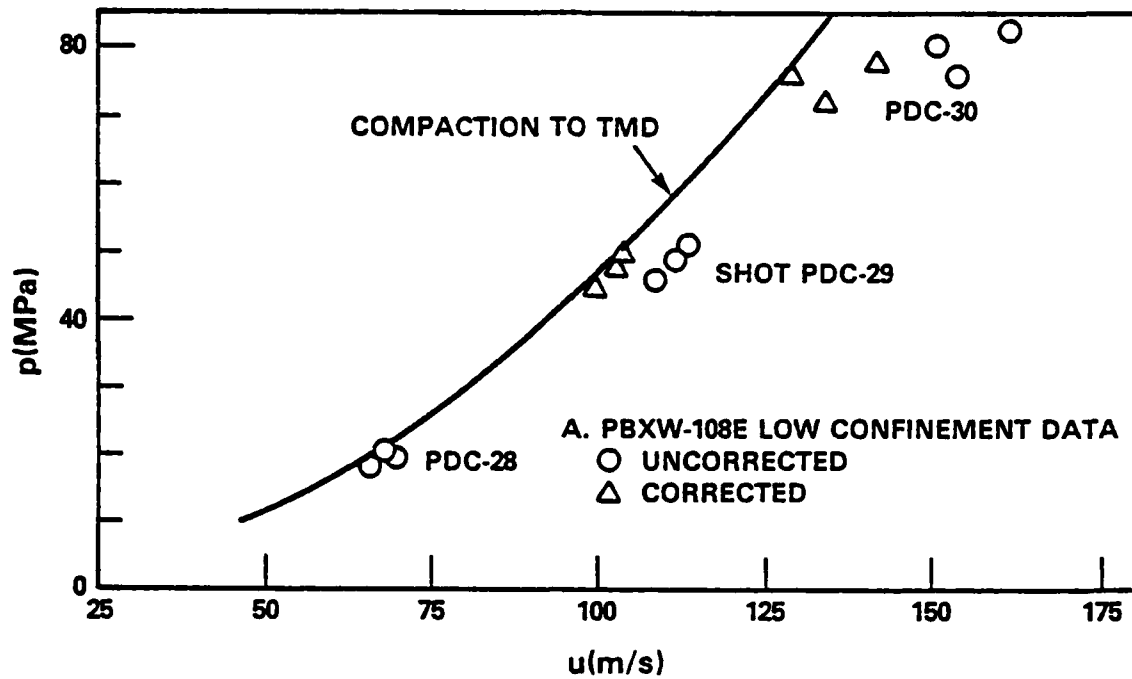


FIGURE 16. PRESSURE VERSUS PARTICLE VELOCITY FOR PISTON DRIVEN COMPACTION OF 75% TMD BEDS OF A. PBXW-108(E) AND B. PBXW-109(E)

CHAPTER 4

SUMMARY AND CONCLUSIONS

Dynamic compaction of high porosity inert and energetic materials was studied for various compaction drivers: pressurized gas, an impacting rod, an accelerating piston, and an explosively driven shock wave. For all of these drivers, as well as for the relatively low (10-15 MPa) pressure generated by a standard NSWC DDT ignitor,⁵ compaction fronts propagate the full length (usually >100 mm) of the porous beds. The compaction waves observed in this study, except for the initial ramping purposely designed into one experiment, were quasi-steady with distinct fronts; as best as could be observed, there was never a two wave structure. In view of the preceding, measurements of particle and compaction front velocity were used in jump condition calculations of pressure and extent of compaction. Although no direct measurements of pressure were available for confirming the calculations, direct measurements of extent of compaction did verify those calculations.

Most measurements were made on porous beds packed in Lexan tubes in order to permit both high-speed photography and flash radiography of the compaction process. However, there was significant yielding of those tubes and a departure from a one-dimensional compaction process for pressures exceeding 25 MPa. The same tube yielding occurs during low confinement DDT experiments. However, for the purpose of comparison with quasi-static compaction measurements and dynamic compaction during high confinement DDT experiments, it was desirable to correct the data for tube expansion. An approximate correction is straightforward, knowing the extent of wall expansion. This expansion was determined from strain gage measurements on the outer wall in some experiments, but had to be calculated in other experiments by assuming that the pressure on the inner wall was the same as the jump pressure (i.e., hydrostatic pressure behind the compaction front). Comparison of corrected data with data from several intermediate confinement experiments indicated that the corrections based on strain gage measurements were reasonable. Assuming hydrostatic pressure was adequate for the PBXs, but resulted in overestimating the wall expansion and the correction for melamine and HMX data. Therefore, it appears that the softer, more pliable materials tend to be more uniformly stressed than the crystalline materials. Some rate dependence probably exists in all of these materials. Relative to the other materials, PBXW-108(E) and 109(E) were easily compacted, achieving TMD for stresses of 40 MPa or less. Except for the PBXs and the inerts, the generation of dynamic compaction data up to pressures of 100 MPa was not possible because of the onset and growth of compressive reaction, which is a direct result of void collapse in the porous beds.

REFERENCES

1. Bernecker, R. R., Sandusky, H. W., and Clairmont, A. R., Jr., "Compaction and the Burning to Detonation Transition at Low Confinement," Proceedings of 16th JANNAF Combustion Meeting, CPIA Publ. 308, Vol. 1, 1979, pp. 91-116.
2. Bernecker, R. R., Sandusky, H. W., and Clairmont, A. R., Jr., "Deflagration-to-Detonation Transition Studies of Porous Explosive Charges in Plastic Tubes," Seventh Symposium (International) on Detonation, NSWC MP 82-334, Naval Surface Weapons Center, 1982, pp. 119-138.
3. Butcher, A. G., Keefe, R. L., Robinson, N. J., and Beckstead, M. W., "Effects of Ignitor and Compaction on DDT Run Up in Plastic Pipes," Seventh Symposium (International) on Detonation, NSWC MP 82-334, Naval Surface Weapons Center, 1982, pp. 143-150.
4. Sandusky, H. W., Elban, W. L., Kim, K., Bernecker, R. R., Gross, S. B., and Clairmont, A. R., Jr., "Compaction of Porous Beds of Inert Materials," Seventh Symposium (International) on Detonation, NSWC MP 82-334, Naval Surface Weapons Center, 1982, pp. 843-856.
5. Sandusky, H. W., Bernecker, R. R., and Clairmont, A. R., Jr., Dynamic Compaction of Inert Porous Beds, NSWC TR 81-97, 31 Oct 1983.
6. Sandusky, H. W., Coffey, C. S., and Liddiard, T. P., "Rate of Deformation as a Measure of Reaction Threshold in Energetic Materials," in Mechanical Properties at High Rates of Strain, 1984 (Bristol: The Institute of Physics, 1984), pp. 373-380.
7. Elban, W. L., Gross, S. B., Kim, K., and Bernecker, R. R., Quasi-Static Compaction Studies for DDT Investigations: Inert Materials, NSWC TR 81-113, 1 Dec 1982.
8. Sandusky, H. W., Elban, W. L., and Liddiard, T. P., "Compaction of Porous Beds," in Shock Waves in Condensed Matter - 1983 (Amsterdam: North Holland, 1984), pp. 567-570.
9. Elban, W. L., "Quasi-Static Compaction Studies for DDT Investigations: Ball Propellants," Propellants, Explosives, and Pyrotechnics, Vol. 9, No. 4, 1984, pp. 119-129.

REFERENCES (Cont.)

10. Elban, W. L. and Chiarito, M. A., "Quasi-Static Compaction Study of Coarse HMX Explosive," to be published in Powder Technology.
11. Coyne, P. J., Jr. and Elban, W. L., "A Strain Rate Sensitivity Prediction for Porous Bed Compaction," in Shock Waves in Condensed Matter - 1983 (Amsterdam: North Holland, 1984), pp. 147-150.
12. Coyne, P. J., Jr., Elban, W. L., and Chiarito, M. A., "The Strain Rate Behavior of Coarse HMX Porous Bed Compaction," to be presented at Eighth Symposium (International) on Detonation, Preprints Vol. 2, 1985, pp. 700-711.
13. Kim, K., "Numerical Simulation of Convective Combustion of Ball Powders in Strong Confinement," AIAA Paper 82-0356, AIAA Journal, Vol. 22, 1984, pp. 793-796.
14. Boggs, T. L., Price, C. F., and Derr, R. L., "Transient Combustion: An Important Consideration in Deflagration-to-Detonation Transition," AGARD Conference Preprint No. 367: Hazard Studies for Solid Propellant Rocket Motors, 1984.
15. Sandusky, H. W., "Compressive Ignition and Burning in Porous Beds of Energetic Materials," Proceedings of the 3rd JANNAF Propulsion System Hazards Subcommittee Meeting, CPIA Publ. 381, Vol. 1, 1983, pp. 249-257.
16. Sandusky, H. W. and Bernecker, R. R., "Compressive Reaction in Porous Beds of Energetic Materials," to be presented at Eighth Symposium (International) on Detonation, Preprints Vol. 2, 1985, pp. 631-640.
17. Green, L. G., James, E., Lee, E. L., Chambers, E. S., Tarver, C. M., Westmoreland, C., Weston, A. M., and Brown, B., "Delayed Detonation in Propellants from Low Velocity Impact," Seventh Symposium (International) on Detonation, NSWC MP 82-334, Naval Surface Weapons Center, 1982, pp. 256-264.
18. Price, D., Bernecker, R. R., Erkman, J. O., and Clairmont, A. R., Jr., DDT Behavior of Tetryl and Picric Acid, NSWC/WOL TR 76-31, 21 May 1976.
19. Jacobs, S. J., McLanahan, J. D., and Whitman, E. C., "A High-Speed Focal-Plane Shutter Framing Camera," Journal of the SMPTE, Vol. 72, No. 12, 1963, pp. 923-926.
20. Bernecker, R. R. and Price, D., Transition from Deflagration to Detonation in Granular Explosives, NOLTR 72-202, 13 Dec 1972.
21. Madigosky, W. M., Shear Modulus and Loss Factor Measurements of Several Explosives and Propellants, NSWC TR 84-246, 25 May 1984.

NOMENCLATURE

Abbreviations:

Al	Aluminum
CF	Compaction front
CGC	Cold gas (gas driven) compaction
DDT	Deflagration-to-detonation transition
HMX	Cyclotetramethylenetetranitramine
IDC	Ignitor driven compaction
NC	Nitrocellulose
NG	Nitroglycerin
PBX	Plastic bonded explosive
PDC	Piston driven compaction
PMMA	Polymethylmethacrylate
RDX	Cyclotrimethylenetrinitramine
RLC	Ramp loaded compaction
SDC	Shock driven compaction
SDT	Shock-to-detonation transition
SG	Strain gage

Physical parameters:

B	Bulk modulus
c_L	Longitudinal wave velocity
c_S	Shear wave velocity
d	Bed or tube diameter
L	Initial bed length
p	Pressure
t	Time
TMD	Theoretical maximum density at ambient pressure
%TMD	Volume percentage of a porous bed that is occupied by solid
u	Particle velocity
U	Wave (CF) velocity
x	Axial distance
Δx	Axial displacement
v_p	Piston velocity prior to impact
δ^p	Average particle size
ϵ_{qs}	Quasi-steady circumferential strain on outer tube wall
ρ	Density

NOMENCLATURE (Cont.)

Subscripts:

c	Compacted
e	Outer tube wall
f	Final
h	As determined by jump conditions
L	Far end of the bed
o	Initial
w	Inner tube wall

DISTRIBUTION

	<u>Copies</u>		<u>Copies</u>
Commander		Commander	
Naval Air Systems Command		Naval Weapons Center	
Attn: AIR-350	1	Attn: Technical Library	1
AIR-324A (B. Sopers)	1	Code 389 (R. Derr)	1
Department of the Navy		Code 3891 (T. Boggs)	1
Washington, DC 20361		Code 3891 (C. Price)	1
		Code 3891 (K. Graham)	1
Commander		China Lake, CA 93555	
Naval Sea Systems Command		Director	
Attn: SEA-99612	2	Naval Research Laboratory	
SEA-62R2	1	Attn: Technical Information	
SEA-62R32	1	Section	2
SEA-06I	1	Washington, DC 20375	
Department of the Navy		Director	
Washington, DC 20362		Defense Advanced Research	
Director		Projects Agency	
Strategic Systems Project		Washington, DC 20301	1
Office (PM-1)		Commanding Officer	
Attn: SP2731 (J. Culver)	1	Naval Weapons Station	
SP273 (E. L. Throckmorton)	1	Attn: R & D Division	1
Department of the Navy		Code 50	1
Washington, DC 20376		Yorktown, VA 23691	
Chief of Naval Research		Air Force Office of Scientific	
ATTN: ONR-1132P (R. Miller)	1	Research	
ONR-741 (Technical Library)	1	ATTN: L. H. Caveny	1
Department of the Navy		Bolling Air Force Base	
Arlington, VA 22217		Washington, DC 20332	
Commanding Officer		Department of the Air Force	
Naval Propellant Plant		AFRPL/DY, Stop 24	
Attn: Technical Library	1	Attn: C. Merrill	1
Indian Head, MD 20640		Edwards AFB, CA 93523	
Office of Naval Technology		Georgia Inst. of Tech.	
ATTN: ONT-071 (E. Zimet)	1	ATTN: Prof. E. Price	1
ONT-0712 (D. Siegel)	1	School of Aerospace Eng.	
Department of the Navy		Atlanta, GA 91125	
800 North Quincy Street			
Arlington, VA 22217			

DISTRIBUTION (Cont.)

	<u>Copies</u>		<u>Copies</u>
Commanding Officer Naval Weapons Evaluation Facility Attn: Code AT-7 Kirtland Air Force Base Albuquerque, NM 87117	1	Armament Development & Test Center DL0SL/Technical Library Eglin Air Force Base, FL 32542	1
Superintendent Naval Academy Attn: Library Annapolis, MD 21402	1	Commanding Officer Naval Ordnance Station Louisville, KY 40124	1
Naval Plant Representative Office Strategic Systems Project Office Lockheed Missiles and Space Co. Attn: SPL-332 P. O. Box 504 Sunnyvale, CA 94088	1	U. S. Department of Energy Attn: DMA Washington, DC 20545	1
AMCRD 5001 Eisenhower Avenue Alexandria, VA 22302	1	Director Applied Physics Laboratory Attn: Library Johns Hopkins Road Laurel, MD 20707	1
Hercules Incorporated Allegany Ballistics Laboratory Attn: Library P. O. Box 210 Cumberland, MD 21502	1	Research Director Pittsburgh Mining and Safety Research Center U. S. Bureau of Mines 4800 Forbes Avenue Pittsburgh, PA 15213	1
Redstone Scientific Information Center U. S. Army Missile Command Attn: Chief, Documents Redstone Arsenal, AL 35809	1	Director Defense Technical Information Center Cameron Station Alexandria, VA 22314	12
Commanding Officer Army Armament Research and Development Command Energetic Materials Division Attn: N. Slagg, DRDAR-LCE Dover, NJ 07801	1	Goddard Space Flight Center, NASA Glenn Dale Road Greenbelt, MD 20771	1
Commanding Officer Harry Diamond Laboratories Attn: Library 2800 Powder Mill Road Adelphi, MD 20783	1	Lawrence Livermore National Laboratory University of California Attn: M. Costantino L. Green E. Lee P. Urtiew C. Tarver P. O. Box 808 Livermore, CA 94550	1 1 1 1 1

DISTRIBUTION (Cont.)

	<u>Copies</u>		<u>Copies</u>
Sandia National Laboratories		SRI International	
Attn: M. Baer		Attn: D. Curran	1
P. Stanton	1	M. Cowperthwaite	1
P. O. Box 5800		333 Ravenswood Avenue	
Albuquerque, NM 87115		Menlo Park, CA 94025	
Director		Teledyne McCormick Selph	
Los Alamos National Laboratory		P. O. Box 6	
Attn: Library	1	Hollister, CA 95023	1
R. L. Rabie	1		
J. Ramsay	1	Lockheed Missiles and Space	
C. Forest	1	Co., Inc.	
A. Bowman	1	P. O. Box 504	
J. McAfee	1	Sunnyvale, CA 94086	1
P. O. Box 1663			
Los Alamos, NM 87544		Rohm and Haas	
Battelle		Huntsville, Defense Contract	
Columbus Laboratories		Office	
ATTN: James H. Adair	1	Attn: H. M. Shuey	1
505 King Avenue		723-A Arcadia Circle	
Columbus, OH 43201		Huntsville, AL 35801	
Chairman		U. S. Army Foreign Service	
DOD Explosives Safety Board		and Technology Center	
Attn: Dr. T. A. Zaker	1	220 7th Street, N. E.	
2461 Eisenhower Avenue		Charlottesville, VA 22901	1
Alexandria, VA 22331			
Aerojet Ordnance and Manufacturing		Princeton Combustion Research	
Company		Laboratories, Inc.	
9236 East Hall Road		1041 U. S. Highway One North	
Downey, CA 90241	1	Attn: M. Summerfield	1
		N. Messina	1
		Princeton, NJ 08540	
Thiokol/Huntsville Division		Pennsylvania State University	
Attn: Technical Library	1	Dept. of Mechanical Engineering	
Huntsville, AL 35807		Attn: K. Kuo	1
Zernow Technical Service Center		University Park, PA 16802	
Attn: Dr. L. Zernow	2	Director	
425 W. Bonita Ave., Suite 208		Ballistic Research Laboratories	
San Dimas, CA 91773		Attn: Library	1
		P. Howe	1
		R. Frey	1
		D. Kooker	1
		Aberdeen Proving Ground, MD 21005	

DISTRIBUTION (Cont.)

	<u>Copies</u>		<u>Copies</u>
Paul Gough Associates 1048 South Street Portsmouth, NH 03801	1	Superintendent Naval Postgraduate School Attn: Library Monterey, CA 93940	1
Hercules Incorporated, Bacchus Works Attn: B. Hopkins	1	Internal Distribution:	
Library 100-H	1	E231	9
D. Caldwell	1	E323	3
K. McCarty	1	R04	1
A. G. Butcher	1	R10	1
P. O. Box 98		R101	1
Magna, UT 84044		R10B	1
		R10C	1
Professor H. Krier		R10D	1
144 MEB, University of IL, at U-C		R10F	2
1206 West Green Street		R11	1
Urbana, IL 61801	1	R11 (M. Kamlet)	1
		R11 (T. Hall)	1
Chemical Propulsion Information Agency		R11 (C. Gotzmer)	1
The Johns Hopkins University		R12	1
Applied Physics Laboratory		R13	1
Johns Hopkins Road		R13 (S. Jacobs)	1
Laurel, MD 20707	1	R13 (D. Price)	1
		R13 (A. Clairmont)	1
IIT Research Institute		R13 (H. Sandusky)	10
Attn: H. S. Napadensky	1	R13 (C. Coffey)	1
10 West 35th Street		R13 (W. Elban)	1
Chicago, IL 60616		R13 (K. Kim)	1
		R13 (J. Forbes)	1
Brigham Young University		R13 (T. Liddiard)	3
Dept. of Chemical Engineering		R13 (V. DeVost)	1
Attn: Dr. M. W. Beckstead	1	R13 (D. Tasker)	1
Provo, UT 84601		R14	1
		R15	1
Library of Congress Attn: Gift and Exchange Division	4		
Washington, DC 20540			
Commanding Officer Naval Underwater Systems Center Attn: LA 151 - Technical Library	1		
Newport, RI 02840			